Quasielastic proton-nucleus scattering in a relativistic plane-wave impulse approximation

C. J. Horowitz
Nuclear Theory Center and Department of Physics, Indiana University, Bloomington, Indiana 47405

D. P. Murdock*
Center for Theoretical Physics, Laboratory for Nuclear Science and Department of Physics, Massachusetts Institute of Technology, Cambridge, Massachusetts 02139
(Received 13 October 1987)

Proton-nucleus quasielastic scattering cross sections and spin observables are calculated in a relativistic plane-wave impulse approximation for nuclei from ^{12}C to ^{208}Pb at energies of 300 to 800 MeV. Relativistic effects are incorporated by using Dirac spinors with enhanced lower components characterized by an effective mass from 0.8 to 0.9M. The analyzing power is found to decrease significantly from free NN values when relativistic spinors are used. This reduction is in good agreement with data. Little change in polarization transfer coefficients $D_{i'j}$ is found at 500 MeV. However, predictions of enhanced $D_{s's}$ and $D_{l'l}$ are made at lower energies. Calculations are also presented for (p,n) quasifree charge exchange reactions. Here the analyzing power is almost unchanged but large changes in cross section and polarization transfer coefficients are possible. These changes depend on how pion contributions to the NN amplitudes are treated. Suggestions for future theoretical and experimental work are made.

I. INTRODUCTION

Most relativistic approaches to nuclear physics suggest the optical potential or self-energy for a nucleon in the nucleus involves large attractive Lorentz scalar and repulsive vector terms.[1-4] For example, relativistic impulse approximation (RIA) calculations[3,4] find strong potentials coming from large scalar and vector pieces of a Lorentz-invariant representation of the NN amplitudes. RIA calculations provide an excellent description of elastic proton scattering. Here, relativity is important because the individual scalar and vector potentials are comparable to the nucleon mass.

However, most of these scattering calculations involve relativistic effects on the projectile in *elastic* scattering. There are many reasons one would like to also examine relativistic effects in inelastic reactions. (a) The reaction content of the RIA is quasifree knockout. Thus, a good description of quasielastic scattering is fundamental to the success of the RIA. (b) Elastic scattering is sensitive to only the scalar and vector pieces of the (isoscalar) NN amplitudes, while inelastic reactions are sensitive to all terms. (c) One would like to examine relativistic effects on nuclear structure as seen through inelastic transitions. (d) Finally, the (p,n) charge-exchange reaction allows one to study relativity in the isovector NN interaction. Relativity may have quite different effects in the isovector channel since here the scalar and vector terms are small while the pseudoscalar invariant (which comes mostly from the pion) is very large.

Elastic scattering from spin-zero targets is sensitive to only the baryon and scalar densities. There have been some relativistic calculations on elastic scattering from polarized nonzero-spin targets.[5,6] This work also attempts to look at other NN amplitudes and further details of nuclear structure. However, recent DWIA calculations[6] show little sensitivity to these ingredients.

In addition, the Colorado group has performed relativistic DWIA calculations to discrete final states. These have been done both with[7] and without[8] an explicit treatment of nucleon exchange, see also Ref. 9. However, transitions to discrete states require relativistic wave functions for the final excited nucleus. Ambiguities in the current very crude wave functions can complicate the interpretation of results.

Here we focus on quasielastic scattering to the continuum with momentum transfer q related to the energy transfer $\omega \approx q^2/2M$. At this high an excitation energy, a simple statistical or Fermi gas model of the target should provide a good first orientation. Indeed, Fermi gas models work well for the gross features of inclusive quasielastic *electron* scattering.[10] In addition, relativistic calculations have been done for electron scattering.[11] However, there appear to be no *spin observables* in the quasifree electron reaction with clear relativistic signatures.

Spin observables in proton scattering may provide uniquely clean data. First, a clear quasifree peak is seen (see Ref. 12, for example) with an excitation energy very close to that for free NN scattering. In addition, the width of the peak agrees well with Fermi motion broadening (except at very large angles). Thus the reaction mechanism is dominated by quasifree scattering. Second, the primary role of distortions on the incoming and outgoing hadron wave functions is to reduce the cross section. Distortions largely cancel in calculating spin observables.[13] Thus spin observables should be insensitive to distortion uncertainties.

Furthermore, all nonrelativistic calculations to date, for example Ref. 14, give essentially the free NN spin observables at the center of the quasielastic peak. The free

NN spin observables thus provide a clear *benchmark* for comparing relativistic calculations and experimental data. Any deviations from the free NN observables are likely to stem from either a change in the collective response of the target (from pionic enhancements, for example) or from a change in the NN interaction in the medium (possibly from relativistic effects). In this work, we show how the strong scalar potential of nuclear field theories influences the NN interaction to give a signature in the quasielastic spin observables.

Relativistic effects are present for the NN interaction in the medium because strong optical potentials enhance the lower components of the Dirac nucleon wave functions. The NN interaction then depends on these wave functions. For example, in relativistic mean field and Brueckner calculations[15,16] the scalar attraction is reduced with respect to the vector repulsion as the wave functions change. Thus, relativistic calculations saturate nuclear matter at a lower density and binding energy than equivalent nonrelativistic calculations (with unchanged four-component spinors). It would be very useful to have experimental information on this important theoretical change in the NN interaction.

Relativistic impulse approximation calculations for elastic scattering[5,17] often use the standard form for the NN amplitudes shown in Table I. This form makes particular predictions for how the NN spin observables depend on the four-component spinors. The five Dirac operators in Table I are used to extrapolate on-shell NN data to an interaction with different wave functions. Clearly this extrapolation must be model dependent. For example, this form implicitly uses a γ_5 form for the pseudoscalar invariant, while at low energy it is important to use a pseudovector form.[18,19] It may be possible to use the spin observables in quasielastic scattering to test the form of the relativistic interaction.

In a previous work,[13] results were presented for scattering from a nucleon at rest. Here we perform a full relativistic plane-wave impulse approximation (RPWIA) calculation and integrate over the Fermi motion of the target nucleons. This allows us to calculate the energy-transfer dependence of quasifree scattering (due to simple kinematics). In Ref. 13, results were only presented for spin observables at the top of the quasielastic peak.

Furthermore, we consider the (p,n) charge-exchange reaction. This depends on relativistic effects in the isovector NN amplitudes. These may be quite different from relativistic effects in the isoscalar interaction which is (primarily) probed in elastic scattering. The isoscalar NN amplitude has strong scalar and vector components (Table I). In contrast, the pseudoscalar invariant (arising primarily from π exchange) dominates the isovector amplitudes. Thus (p,n) scattering is sensitive to the pseudoscalar invariant and the way in which the pion is treated.

TABLE I. Form of the relativistic NN amplitude used in the text.

$$\hat{\mathcal{F}}=\sum_i F^i(q,E)\lambda^i_{(1)}\lambda^i_{(2)}$$

i	λ^i
S (scalar)	1
V (vector)	γ_μ
P (pseudoscalar)	γ_5
A (axial vector)	$\gamma_5\gamma_\mu$
T (tensor)	$\sigma_{\mu\nu}$

Finally, in this paper we use different Dirac spinors for the projectile and target. This allows us to examine separately relativistic effects on the projectile and the nuclear structure of the target. It has been claimed that elastic scattering is primarily sensitive to relativistic effects on the projectile rather than the target.[20]

In Sec. II the RPWIA formalism is developed to calculate cross sections and spin observables assuming a Fermi gas for the target; a number of the approximations which we use are then discussed. Section III presents results for cross sections and spin observables from a variety of targets (^{12}C to ^{208}Pb) at laboratory kinetic energies $T_{\rm lab}$ from 200 to 800 MeV. Here special attention is paid to the 500 MeV LAMPF experiment.[21] Finally, Sec. IV presents conclusions and discusses further experimental and theoretical work.

II. RELATIVISTIC PWIA

A. Formalism

In this section we calculate spin observables in a relativistic plane-wave impulse approximation (RPWIA) assuming a Fermi gas model for the target. First, we discuss projectile and target wave functions at an appropriate average density. Then the square of the scattering matrix element is written with spin projection operators. Next, traces are taken to calculate cross sections and spin observables. Finally, a numerical integration is performed over the Fermi motion of the target nucleons. This involves interpolating the experimental NN amplitudes over a range of effective energies. We close this section by considering the (p,n) reaction.

We begin by considering uniform nuclear matter with appropriate four-component spinors for the projectile and target nucleons. The use of a local density approximation for finite nuclei will be discussed later. The spinors are solutions to a Dirac equation in an optical potential $U(r,E)$ which in general depends on both position and energy:

$$U(r,E)=S(r,E)+\gamma_0 V(r,E)\ . \tag{2.1}$$

Here γ_0 is a Dirac matrix (our conventions are those of Ref. 22) and S is the scalar and V the vector potentials. We assume S and V are approximately proportional to the baryon density:

$$S(r,E)\approx S_0(E)\frac{\rho(r)}{\rho_0}\ . \tag{2.2}$$

Here $S_0(E)$ is the strength at the origin where the density is ρ_0.

As a first cut we simply evaluate Eq. (2.2) at an average density $\langle\rho\rangle$ appropriate for the surface-peaked reaction:

$$\langle\rho\rangle=\frac{\int b\,db\,T(b)\int dz\,\rho(b,z)^2}{\int b\,db\,T(b)\int dz\,\rho(b,z)}\ , \qquad k_F=(\tfrac{3}{2}\pi^2\langle\rho\rangle)^{1/3}\ . \tag{2.3}$$

In Eq. (2.3), an eikonal approximation is assumed; $T(b,E)$ is the transmission probability for going through the nucleus at impact parameter b with energy E, and z is the coordinate along the incident beam. We will drop spin-orbit and Darwin terms when evaluating T and hence in the calculation of the spin observables; later, in Sec. III we estimate the effect of the L·S term. Thus, we use

$$T(b,E)=\exp\left[\frac{4M}{k}\int_0^\infty dz\ \mathrm{Im}V_c(b,z)\right]\ , \tag{2.4}$$

where V_c is the Schrödinger-equivalent central potential

$$V_c=S+\frac{E}{M}V+\frac{1}{2M}(S^2-V^2)\ . \tag{2.5}$$

[Note, Eq. (2.3) gives results similar to the slightly different definition used in Ref. 13.] Using Eq. (2.3) we define an average scalar field $\bar{S}(E)$:

$$\bar{S}(E)=S_0(E)\frac{\langle\rho\rangle}{\rho_0}\ . \tag{2.6}$$

The four-component spinor for the projectile of momentum $\mathbf{p}_1$ in these potentials is

$$U_1(\mathbf{p}_1)=\left[\frac{E_1^*+M_1}{2M_1}\right]^{1/2}\begin{bmatrix}1\\ \dfrac{\boldsymbol{\sigma}\cdot\mathbf{p}_1}{E_1^*+M_1}\end{bmatrix}\chi_1\ . \tag{2.7}$$

Here χ_1 is a Pauli spinor of projection s_1,

$$E_1^*=(\mathbf{p}_1^2+M_1^2)^{1/2} \tag{2.8}$$

and the effective mass M_1 for the projectile is

$$M_1=M+\bar{S}(E)\ . \tag{2.9}$$

The spinor in Eq. (2.7) is *parametrized* by the mass M_1. That is, M_1 determines the ratio of lower components to upper for a given $\mathbf{p}_1$. As M_1 decreases, the lower components are significantly enhanced. Note, Eq. (2.7) is independent of $V(r,E)$.

The definition of effective mass in Eq. (2.9) is different from the traditional nonrelativistic definition based on the derivative of a spectrum with respect to momentum. Typical values of M_1 are $0.8-0.9M$; see Table II.

For the target nucleon of momentum $\mathbf{p}_2$ we use a different effective mass M_2:

$$M_2=M+\bar{S}_{\mathrm{mft}}(E)\ , \tag{2.10}$$

$$\bar{S}_{\mathrm{mft}}(E)=S_{\mathrm{mft}}\frac{\langle\rho\rangle}{\rho_0}\ , \tag{2.11}$$

$$S_{\mathrm{mft}}=-0.44M\ . \tag{2.12}$$

The scalar potential S_{mft} is taken from Walecka's mean

TABLE II. Average masses, Fermi momenta, and nucleon numbers. The "(e,e')" entries are described in the text.

Target	T_{lab} (MeV)	M_1/M	M_2/M	k_F (fm^{-1})	A_{eff}
^{12}C	200	0.85	0.84	0.97	4.33
^{12}C	400	0.86	0.84	0.98	4.63
^{12}C	500	0.91	0.87	0.91	2.86
^{12}C	800	0.92	0.90	0.83	1.97
^{12}C	(e,e')		0.79	1.06	12
^{40}Ca	200	0.82	0.81	1.04	8.53
^{40}Ca	400	0.83	0.80	1.05	9.70
^{40}Ca	500	0.90	0.85	0.94	6.01
^{40}Ca	800	0.91	0.89	0.85	4.25
^{40}Ca	(e,e')		0.73	1.16	40
^{208}Pb	200	0.82	0.82	1.02	12.44
^{208}Pb	400	0.86	0.83	0.98	12.81
^{208}Pb	500	0.88	0.85	0.95	11.86
^{208}Pb	800	0.82	0.82	1.02	12.44
^{208}Pb	(e,e')		0.66	1.25	208

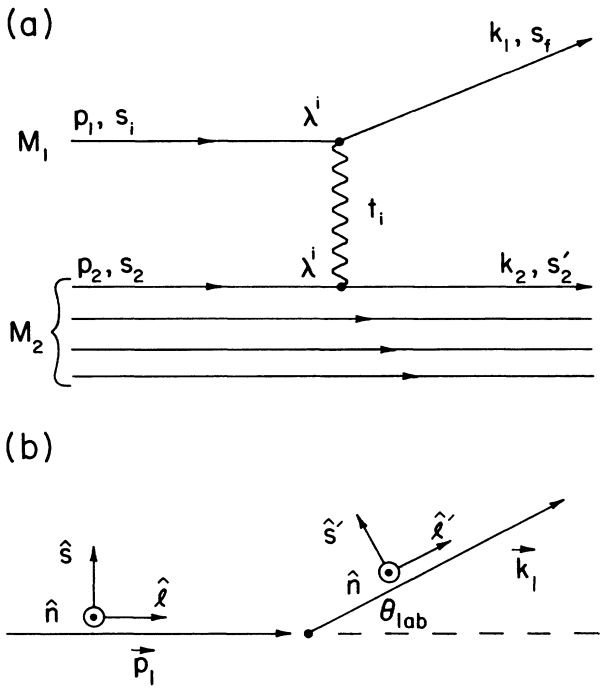

FIG. 1. (a) Schematic diagram of the impulse approximation for quasielastic proton scattering. The index i is summed over the five invariant amplitudes in Table I. (b) Definition of the spin polarization directions $\hat{n}, \hat{s}, \hat{l}, \hat{s}'$, and $\hat{l}'$; see Eq. (2.30a).

field theory[2,23] which has $M^* \approx 0.56M$ at ρ_0. Below, we will use the different M_1, M_2 to examine separately relativistic effects on the projectile and the nuclear structure of the target. Due to the small energy dependence of $S(r,E)$ we note that M_1 is slightly larger than M_2.

Consider the scattering of a projectile by a target nucleon as shown in Fig. 1(a). The invariant matrix element for this process is given by

$$\mathcal{M} = \sum_{i=S}^{T} \bar{U}_1(k_1,s_f)\lambda^i U_1(p_1,s_i) t_i(q,T_{\text{eff}}) \times \bar{U}_2(k_2,s')\lambda^i U_2(p_2,s) , \tag{2.13}$$

where we use the conventions of Bjorken and Drell.[22] Here the $t_i(q,T_{\text{eff}})$ are simply related by kinematic factors to the NN amplitudes F_i and Dirac operators λ^i of Ref. 3 and given in Table I:

$$t_i(q,T_{\text{eff}}) = \frac{8\pi k_{\text{eff}} E_{\text{eff}}}{M^2} F_i(q,T_{\text{eff}}) . \tag{2.14}$$

We note that $t_i(q,T_{\text{eff}})$ involves the full antisymmetrized NN amplitude; no attempt has been made to separate it into direct and exchange pieces (see Ref. 24, for example). This approximation should be good at high energy $T_{\text{lab}} \geq 500$ MeV, but at lower energies $T_{\text{lab}} \approx 200$ MeV a better treatment of exchange may be needed. The effective laboratory kinetic energy T_{eff} at which the NN amplitudes will be evaluated is discussed below (along with the factors k_{eff} and E_{eff}).

Squaring $\mathcal{M}$ and summing over the unobserved spin of the target nucleon, one has

$$\sum_{s_2,s_2'} \mathcal{M}^*\mathcal{M} = \sum_{i,j=S}^{T} \text{Tr}_1 \left[\frac{\not{k}_1 + M_1}{2M_1} \left[\frac{1+\gamma_5 \not{s}_f}{2} \right] \lambda_j \frac{\not{p}_1 + M_1}{2M_1} \left[\frac{1+\gamma_5 \not{s}_i}{2} \right] \lambda_i \right] \text{Tr}_2 \left[\frac{\not{k}_2 + M_2}{2M_2} \lambda_j \frac{\not{p}_2 + M_2}{2M_2} \lambda_i \right] t_i^* t_j . \tag{2.15}$$

Here we used

$$\sum_s U_2(k_2,s)\bar{U}_2(k_2,s) = \frac{\not{k}_2 + M_2}{2M_2} \tag{2.16}$$

and

$$U_1(k,s)\bar{U}_1(k,s) = \frac{\not{k} + M_1}{2M_1} \left[\frac{1+\gamma_5 \not{s}}{2} \right] , \tag{2.17}$$

where the spin four-vector s satisfies $s^2 = -1$ and

$$s_f \cdot k_1 = s_i \cdot p_1 = 0 . \tag{2.18}$$

The cross section *per target nucleon* is calculated from Eq. (2.15) and the appropriate kinematic factors. The cross section is simply averaged over a Fermi gas momentum distribution for p_2 up to k_F. As in Ref. 22 we have

$$d\sigma = \frac{1}{|\mathbf{v}_1 - \mathbf{v}_2|} \frac{M_1^2}{E_1^* E_1^{*\prime}} \int_{p_2 \leq k_F} \frac{d^3p_2}{\frac{4}{3}\pi k_F^3} \frac{M_2^2}{E_2^* E_2^{*\prime}} \frac{d^3k_1}{(2\pi)^2} \delta(E_1^* + E_2^* - E_1^{*\prime} - E_2^{*\prime}) \sum_{s_i,s_f,s_2,s_2'} \tfrac{1}{4}\mathcal{M}^*\mathcal{M} . \tag{2.19}$$

Here the target recoil momentum is

$$\mathbf{k}_2=\mathbf{p}_1+\mathbf{p}_2-\mathbf{k}_1 \tag{2.20}$$

with $\mathbf{k}_1$ the final momentum of the projectile. Also,

$$\begin{aligned} E_1^*&=(\mathbf{p}_1^2+M_1^2)^{1/2},\quad E_1^{*\prime}=(\mathbf{k}_1^2+M_1^2)^{1/2}\ , \\ E_2^*&=(\mathbf{p}_2^2+M_2^2)^{1/2},\quad E_2^{*\prime}=(\mathbf{k}_2^2+M_2^2)^{1/2}\ . \end{aligned} \tag{2.21}$$

Next, the double differential cross section is calculated starting from

$$d^3k_1=k_1E_1'dE_1'd\Omega_1'\ , \tag{2.22}$$

where the experimentally detected final energy

$$E_1'=(\mathbf{k}_1^2+M^2)^{1/2}$$

is related to the final momentum $\mathbf{k}_1$. The incident flux is evaluated approximately in nuclear matter:

$$|\mathbf{v}_1-\mathbf{v}_2|\approx\frac{|\mathbf{p}_1|}{E_1^*}\ . \tag{2.23}$$

This gives

$$\frac{d^3\sigma}{d\Omega_1'dE_1'}=\int_{p_2\le k_F}d^3p_2\theta\sum_{s_2,s_2',s_i,s_f}\tfrac{1}{4}\mathcal{M}^*\mathcal{M}\ , \tag{2.24a}$$

where

$$\theta=\frac{k_1}{p_1}M_1^2\frac{E_1'}{E_1^{*\prime}}\frac{1}{\frac{4}{3}\pi k_F^3}\frac{M_2^2}{E_2^*E_2^{*\prime}}\frac{\delta(E_1^*+E_2^*-E_2^{*\prime}-E_1^{*\prime})}{(2\pi)^2}\ , \tag{2.24b}$$

The total scattering from $Z_{\rm eff}$ protons and $N_{\rm eff}$ neutrons is assumed to be

$$\frac{d^3\sigma}{d\Omega_1'dE_1'}=Z_{\rm eff}\frac{d^3\sigma({\rm pp})}{d\Omega_1'dE_1'}+N_{\rm eff}\frac{d^3\sigma({\rm pn})}{d\Omega_1'dE_1'}\ . \tag{2.25}$$

Here $d^3\sigma({\rm pp})/d\Omega_1'dE_1'$ is obtained from Eq. (2.24) evaluated using the proton-proton amplitudes while $d\sigma({\rm pn})/d\Omega_1'dE_1'$ uses the proton-neutron amplitudes. We discuss the calculation of the effective number of nucleons $N_{\rm eff}$ and $Z_{\rm eff}$ below. (We assume the same k_F for both neutrons and protons.)

The traces in Eq. (2.15) has been evaluated with a computer algebra program. The spin-independent cross section comes from

$$\begin{aligned} \sum_{s_2,s_2',s_i,s_f}\mathcal{M}^*\mathcal{M}=&\,t_S^*t_S(1+K_1\cdot P_1)(1+K_2\cdot P_2)+t_P^*t_P(1-K_1\cdot P_1)(1-K_2\cdot P_2) \\ &+2t_V^*t_V(2-K_1\cdot P_1-K_2\cdot P_2+K_1\cdot K_2P_1\cdot P_2+K_1\cdot P_2K_2\cdot P_1) \\ &+2t_A^*t_A(2+K_1\cdot P_1+K_2\cdot P_2+K_1\cdot K_2P_1\cdot P_2+K_1\cdot P_2K_2\cdot P_1) \\ &+8t_T^*t_T(3-K_1\cdot P_1K_2\cdot P_2+2K_1\cdot K_2P_1\cdot P_2+2K_1\cdot P_2K_2\cdot P_1) \\ &+2\,{\rm Re}(t_V^*t_S-6t_T^*t_A)(K_1\cdot K_2+K_1\cdot P_2+K_2\cdot P_1+P_1\cdot P_2) \\ &-2\,{\rm Re}(t_A^*t_P-6t_T^*t_V)(K_2\cdot P_1+K_1\cdot P_2-K_1\cdot K_2-P_1\cdot P_2) \\ &+4\,{\rm Re}(t_A^*t_V-t_T^*t_S-t_T^*t_P)(K_1\cdot K_2P_1\cdot P_2-K_2\cdot P_1K_1\cdot P_2)\ , \end{aligned} \tag{2.26}$$

where $K_i=k_i/M_i$ and $P_i=p_i/M_i$.

The polarization (which is equal to the analyzing power in this approximation to quasifree scattering) is calculated by summing over the initial spin of the projectile but not its final spin:

$$\begin{aligned} \sum_{s_i,s_2,s_2'}\mathcal{M}^*\mathcal{M}=&\,{\rm Im}\left[t_S^*t_V+2t_T^*t_A-\frac{M_1}{M_2}(t_A^*t_V+2t_T^*t_S)\right] \\ &\times[(E_2^*+E_2^{*\prime})\mathbf{p}_1\times\mathbf{k}_1+E_1^*\mathbf{k}_1\times(\mathbf{p}_2+\mathbf{k}_2)-E_1^{*\prime}\mathbf{p}_1\times(\mathbf{p}_2+\mathbf{k}_2)]\cdot\frac{\mathbf{s}_f}{M_1^2M_2}\ . \end{aligned} \tag{2.27}$$

This is dominated by the interference of the vector and scalar amplitudes. Thus the analyzing power is relatively simple when the NN amplitudes are written in terms of the Lorentz invariants of Table I. Furthermore, there are no sensitive cancellations between different NN amplitudes.

The analyzing power per target proton $A_y({\rm pp})$ equals the polarization P, which is given by

$$A_y({\rm pp})=P({\rm pp})=\frac{\int_{p_2\le k_F}d^3p_2\theta\frac{1}{4}\sum_{s_i,s_2,s_2'}[\mathcal{M}^*\mathcal{M}(\mathbf{s}_f=\hat{n},{\rm pp})-\mathcal{M}^*\mathcal{M}(\mathbf{s}_f=-\hat{n},{\rm pp})]}{(d^3\sigma/d\Omega_1'dE_1')({\rm pp})} \tag{2.28}$$

with a similar expression for $A_y({\rm pn})$ for scattering from target neutrons, which involves $\mathcal{M}^*\mathcal{M}({\rm pn})$. Here, $\hat{n}$ is the normal to the reaction plane; see Eq. (2.30b). The total analyzing power is then

$$A_y=\left[Z_{\rm eff}\frac{d^3\sigma({\rm pp})}{d\Omega_1'dE_1'}A_y({\rm pp})+N_{\rm eff}\frac{d^3\sigma({\rm pn})}{d\Omega_1'dE_1'}A_y({\rm pn})\right]\Big/\frac{d^3\sigma}{d\Omega_1'dE_1'}\ . \tag{2.29}$$

The polarization transfer observables $D_{i'j}$ are obtained from the full trace in Eq. (2.15), which is given in the Appendix. The $D_{i'j}$ describe the scattering of a proton with spin in the $\hat{j}$ direction ($\hat{j}$=one of $\hat{n}$, $\hat{l}$, or $\hat{s}$) to spin in the $\hat{i}'$ direction ($\hat{i}'=\hat{n}$, $\hat{l}'$, or $\hat{s}'$). The $D_{i'j}$ (per proton) are given by

$$M_{i'j}=\tfrac{1}{4}\sum_{s_2,s_2'}[\mathcal{M}^*\mathcal{M}(\mathbf{s}_i=\hat{j},\mathbf{s}_f=\hat{i}')-\mathcal{M}^*\mathcal{M}(\mathbf{s}_i=\hat{j},\mathbf{s}_f=-\hat{i}')-\mathcal{M}^*\mathcal{M}(\mathbf{s}_i=-\hat{j},\mathbf{s}_f=\hat{i}')+\mathcal{M}^*\mathcal{M}(\mathbf{s}_i=-\hat{j},\mathbf{s}_f=-\hat{i}')]\ ,$$

$$D_{i'j}(\mathrm{pp})=\int_{p_2\le k_F}d^3p_2\theta M_{i'j}(\mathrm{pp})\Big/\frac{d^3\sigma(\mathrm{pp})}{d\Omega_1'dE_1'}\ , \tag{2.30a}$$

where the coordinate system is

$$\hat{n}=\frac{\mathbf{p}_1\times\mathbf{k}_1}{|\mathbf{p}_1\times\mathbf{k}_1|},\quad \hat{l}=\hat{p}_1,\quad \hat{s}=\hat{n}\times\hat{p}_1,\quad \hat{l}'=\hat{k}_1,\quad \hat{s}'=\hat{n}\times\hat{k}_1\ . \tag{2.30b}$$

Here $\mathbf{p}_1$ is the initial and $\mathbf{k}_1$ is the final projectile laboratory momentum; see Fig. 1(b). Thus $\hat{l}$ is the initial "longitudinal" and $\hat{s}$ the "sideways" direction. (Because of parity and time reversal invariance, there are only five nonzero $D_{i'j}$: $D_{l'l}$, $D_{s's}$, D_{nn}, $D_{s'l}$, and $D_{l's}$.) We then form an appropriate isospin sum like Eq. (2.29).

$$D_{i'j}=\left[Z_{\mathrm{eff}}\frac{d^3\sigma(\mathrm{pp})}{d\Omega_1'dE_1'}D_{i'j}(\mathrm{pp})+N_{\mathrm{eff}}\frac{d^3\sigma(\mathrm{pn})}{d\Omega_1'dE_1'}D_{i'j}(\mathrm{pn})\right]\Big/\frac{d^3\sigma}{d\Omega_1'dE_1'}\ . \tag{2.31}$$

The integral over d^3p_2 is evaluated as follows:

$$\int d^3p_2\delta(E_1^*+E_2^*-E_2^{*\prime}-E_1^{*\prime})=\int_{p_{\min}}^{k_F}dp_2\frac{p_2E_2^{*\prime}}{q}\int d\phi\,|_{\chi=\chi_0}\ . \tag{2.32}$$

Here the angle χ between $\mathbf{p}_2$ and $\mathbf{q}$ is fixed by the energy-conserving δ function:

$$\cos\chi=\cos\chi_0=\frac{q_\mu^2+2\omega E_2^*}{2p_2q}\ , \tag{2.33}$$

where the four-momentum transfer is

$$\mathbf{q}=\mathbf{k}_2-\mathbf{p}_2=\mathbf{p}_1-\mathbf{k}_1\ ,$$
$$\omega=E_2^{*\prime}-E_2^*=E_1^*-E_1^{*\prime}\ . \tag{2.34}$$

The minimum momentum of the target nucleon is

$$P_{\min}=\left|\frac{q}{2}-\frac{\omega}{2}\left[1-\frac{4M_2^2}{q_\mu^2}\right]^{1/2}\right|\ . \tag{2.35}$$

If $P_{\min}>k_F$, the cross section is zero. The integrals over p_2 and ϕ (the azimuthal angle of $\mathbf{p}_2$ with respect to $\mathbf{q}$) in Eqs. (2.28)–(2.30) are evaluated numerically. Typically, ten Gaussian points in each integral gave better than 1% accuracy for the spin observables. (In practice, $\mathbf{p}_2$ was generated in a frame with $\mathbf{q}$ along the z axis and then rotated into a frame with $\mathbf{p}_1$ along the z axis.)

For each p_2 and ϕ, the NN amplitudes are evaluated at an effective laboratory kinetic energy T_{eff}:

$$T_{\mathrm{eff}}=\frac{E_1E_2-\mathbf{p}_1\cdot\mathbf{p}_2-M^2}{M}\ . \tag{2.36}$$

This equation is the equivalent laboratory energy of a projectile scattering on a nucleon at rest for two *free* nucleons of momenta $\mathbf{p}_1$ and $\mathbf{p}_2$. Note that although we change the four-component spinors (which are parametrized by an M^*) we assume the momenta of the initial and final projectile are equal to their free values. Any change in momenta would be governed by the real part of V_c in Eq. (2.5). For T_{lab} around 400 MeV, V_c is going through zero and is only slightly repulsive in the interior. Furthermore, V_c has a wine-bottle-bottom shape [from the quadratic terms in Eq. (2.5)] with a small pocket of attraction in the surface and a radial node. Thus we expect V_c to have only a small average effect on the surface-peaked reaction (see also Ref. 13). The NN amplitudes are also evaluated at an effective center of mass scattering angle $\theta_{\mathrm{eff}}^{\mathrm{c.m.}}$ given by

$$\theta_{\mathrm{eff}}^{\mathrm{c.m.}}=2\arcsin\left[\frac{-q_\mu^2}{2MT_{\mathrm{eff}}}\right]^{1/2}\ . \tag{2.37}$$

This just assures that the four momentum transfer is q. Similarly, k_{eff} and E_{eff} in Eq. (2.14) are the momentum and energy in the effective lab frame:

$$E_{\mathrm{eff}}=T_{\mathrm{eff}}+M=(k_{\mathrm{eff}}^2+M^2)^{1/2}\ .$$

In practice, a large table of relativistic invariant amplitudes calculated from the SM86 Arndt phase shifts[25] (with the Coulomb interaction removed) is interpolated on both T_{eff} and $\theta_{\mathrm{eff}}^{\mathrm{c.m.}}$. Here some care is needed because of the sensitive cancellations between different Lorentz invariant amplitudes. The calculations in Sec. III use quadratic interpolation every 25 MeV on T_{eff} and linear interpolation every 5 degrees on $\theta_{\mathrm{c.m.}}$.

For (p,n) charge-exchange reactions we set $Z_{\mathrm{eff}}=0$ and replace F_{pn} with the isovector (charge-exchange) amplitudes $F_{\mathrm{ch\text{-}ex}}$:

$$F_{\mathrm{ch\text{-}ex}}=F_{\mathrm{pp}}-F_{\mathrm{pn}}\ . \tag{2.38}$$

The Lorentz character of the isovector amplitudes is radically different from the isoscalar amplitudes F_{av},

$$F_{\rm av}=F_{\rm pp}+F_{\rm pn}\ , \tag{2.39}$$

as discussed in Sec. III.

The cross section depends on the effective number of protons $Z_{\rm eff}$ and neutrons $N_{\rm eff}$; these are calculated from a simple eikonal estimate of the effective number of nucleons $A_{\rm eff}$:

$$A_{\rm eff}=\frac{\int b\,db\,T(b)\int dz\,\rho(b,z)}{\int b\,db\int dz\,\rho(b,z)}A\ , \tag{2.40}$$

and we assume

$$Z_{\rm eff}=\frac{Z}{A}A_{\rm eff},\quad N_{\rm eff}=\frac{N}{A}A_{\rm eff}\ . \tag{2.41}$$

Values for $A_{\rm eff}$ are collected in Table II. We note they are greatly reduced from A and depend on energy, being over twice as big at $T_{\rm lab}=400$ as at 800 MeV. [We neglect the small spin-orbit and Darwin parts[26] of V_c when calculating $A_{\rm eff}$; see Eqs. (2.4) and (2.5).]

To summarize, the calculations are based on a Fermi gas of density $\langle\rho\rangle$, Eq. (2.3), with projectile and target wave functions characterized by M_1, Eq. (2.9), and M_2, Eq. (2.11). The cross section is calculated from a numerical integration over p_2 in Eqs. (2.24) and (2.32) using Arndt NN amplitudes at effective energies given by Eq. (2.36). Finally, the analyzing power is calculated from Eqs. (2.27)–(2.29) and the polarization-transfer coefficients $D_{i'j}$ from Eqs. (2.30) and (2.31).

B. Discussion of approximations

In this section we discuss a number of our approximations. First, the effects of spin-orbit distortions are considered. Next, we consider background from multiple scattering.

The dominant effect of our optical distortions is to reduce the cross section [which we include through $A_{\rm eff}$, Eq. (2.40)] without changing spin observables. However, any spin dependence of the distortions will affect the spin observables. In an eikonal approximation the $\mathbf{L}\cdot\mathbf{S}$ optical potential can rotate the spin of the projectile and mix the different $D_{i'j}$. This effect has been estimated in Ref. 13 to be small, typically 10% or less (see Fig. 5).

However, the $\mathbf{L}\cdot\mathbf{S}$ estimates of Ref. 13 may only be valid near the center of the quasielastic peak. Off the quasielastic peak, it may be favorable to transfer some energy into the distortions and have a hard scattering closer to the center of the peak. This may lead to larger distortion effects on the spin observables; see also Ref. 14. Thus, while distortion may not change observables at the peak, they may change the slope of a spin observable with respect to the excitation energy. Full relativistic DWIA calculations would be very useful to investigate this.

Background from multiple scattering (where two or more hard collisions take place) has been examined by Smith and Wallace.[14] They find that at the quasielastic peak, contributions from two hard scatterings are less than 10% in the cross section and even less in the spin observables. However, far out on the high-energy-loss side of the peak, multiple scattering can be important and substantially reduce spin observables.

III. RESULTS

In this section we present results for cross sections and spin observables using the RPWIA formalism of Sec. II. All calculations use the effective masses and Fermi momenta in Table II. First, cross sections at $T_{\rm lab}=800$ MeV are compared to the extensive LAMPF (Ref. 12) data. Next, spin observables at $T_{\rm lab}=500$ MeV are compared to the recent experiments[21] on Pb and Ca. Predictions are then made for spin observables at other energies and angles. Finally, calculations are presented for the (p,n) charge-exchange reaction, and we close by examining the local density approximation.

A. 800 MeV (p,p')

The cross sections for $T_{\rm lab}=800$ MeV scattering from ^{12}C, ^{40}Ca, and ^{208}Pb are shown in Figs. 2–4. The absolute normalization of the cross section is based on the $A_{\rm eff}$ values in Table II [Eq. (2.40)] and has *not* been adjusted. [Note, the normalization of the data from Ref. 12 has been questioned by up to 25%.[27]] First, the magnitude of the cross sections agrees with the simple $A_{\rm eff}$ to typically 20–40 %, except at very large or small angles. Second, the data clearly show a parabolic quasielastic peak whose position and width agree reasonably well with the calculations (especially for the lighter nuclei and moderate scattering angles). Finally, the cross section data shows a small amount of strength at both higher and lower excitation energies that is not reproduced by the theory. This may be due to nuclear structure effects and multiple scattering.

Calculations are shown in Figs. 2–4 both with *free* wave functions, using $M_1=M_2=M$ (solid lines) and with wave functions characterized by the M^*'s of Table II which include relativistic effects (dashed curves). The magnitude of the cross section is very similar in each case. As M_1 and M_2 decrease, the square of the invariant matrix element $\mathcal{M}^*\mathcal{M}$ increases but the kinematic factors in front in Eq. (2.19) decrease, leaving the cross section almost unchanged. Note, the discussion of "cross sections" in Ref. 13 ignored the kinematic factors and thus is somewhat misleading. [Although correct as written, Eq. (21) of Ref. 13 is not an observable in the medium.]

The position of the quasielastic peak is essentially

$$\omega=(\mathbf{q}^2+M_2^2)^{1/2}-M_2\ . \tag{3.1}$$

This assumes the vector potential is independent of energy—so that it cancels in (3.1)–and that M_2 is also energy independent. This should be a good approximation up to $\omega\approx 200$ MeV. Beyond this energy, the optical potential V_c in Eq. (2.5) with constant S and V is too repulsive. Therefore, optical fits to elastic data[28] above $T_{\rm lab}=200$ MeV have S and V both decreasing with energy. This decreases the large ω predicted by Eq. (3.1) at very large q.

Compared to free NN kinematics, Eq. (3.1) implies a "binding energy shift" of the peak:

$$\Delta E=(\mathbf{q}^2+M_2^2)^{1/2}-(\mathbf{q}^2+M^2)^{1/2}-M_2+M\ . \tag{3.2}$$

Thus the dotted curves (with relativistic effects) are shift-

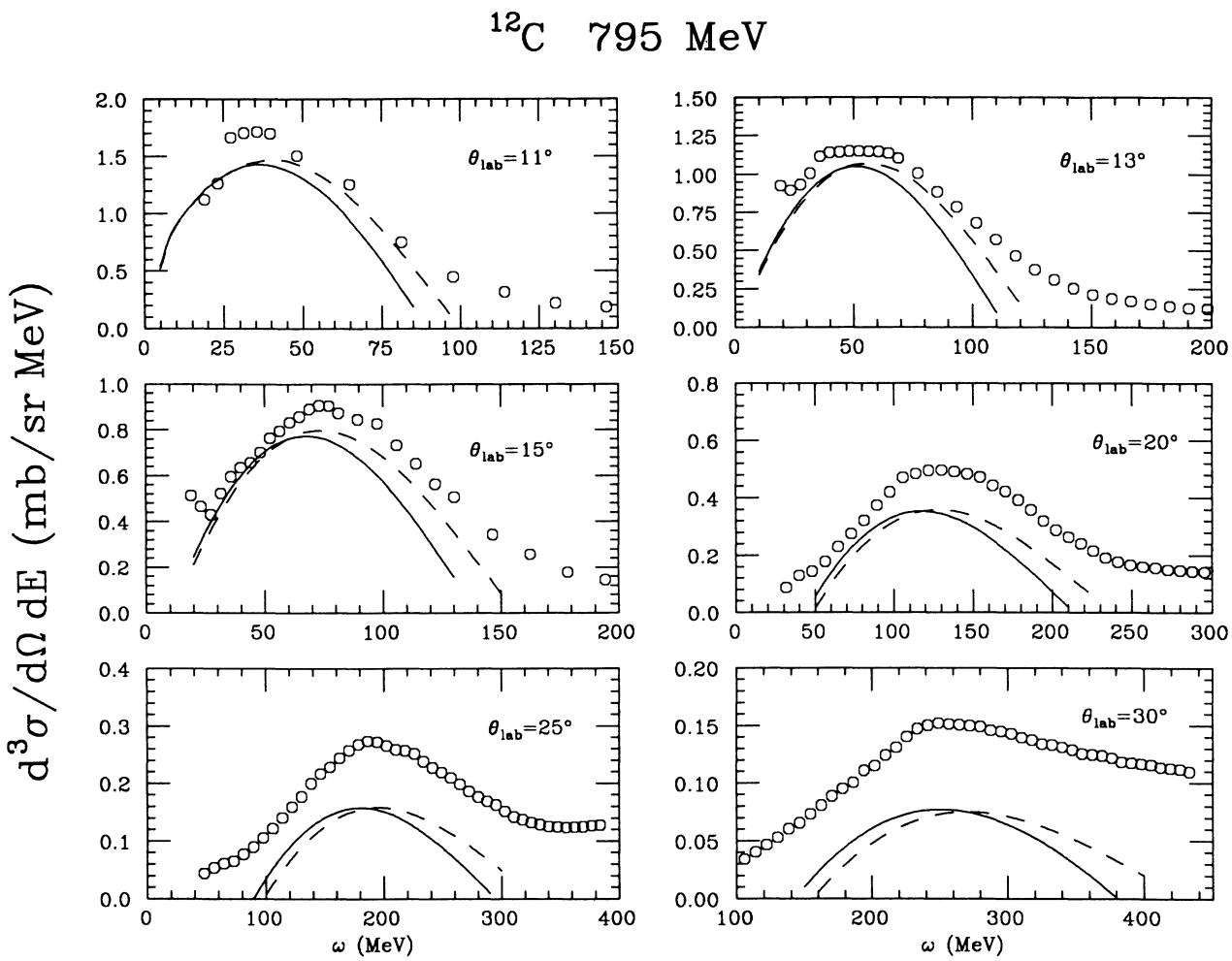

FIG. 2. Cross section vs energy loss for (p,p′) scattering on ^{12}C at 795 MeV and various scattering angles. The solid curves use $M_1=M_2=M$. The dashed curves use effective relativistic masses for M_1 and M_2. Data are from Chrien *et al.*, Ref. 12.

ed to *slightly* higher ω than the free solid curves in Figs. 2–4. Typically, this shift is 10 MeV or less. The small energy shift often leads to slightly better agreement with data for the $M_2 \neq M$ calculation. However, the difference is so slight that the data is consistent with (or without) the shift. We conclude that there are no clear relativistic signatures in the cross section.

The binding energy shift is much smaller than that observed in *electron* scattering. For electron scattering we set $T(b)$ equal to unity in Eq. (2.3) to calculate an appropriate M_2. These values (Table II) are significantly smaller than for the surface-peaked proton reaction. Rosenfelder[10] found a relativistic Fermi gas with $\langle M^* \rangle = 0.71M$ provided a good description of 500 MeV electron scattering from ^{40}Ca. This value is in good agreement with our $M_2 = 0.73M$ from Table II. Thus, our very simple model can describe both the small (or zero) binding shift in proton scattering and the much larger shift in electron scattering.

On the other hand, many nonrelativistic models attribute the observed binding shift in electron scattering to an average shell-model binding energy. They then predict the *same* binding energy shift for proton scattering. This substantially overestimates the very small observed proton shift.

B. 300–500 MeV (p,p′)

We now turn to the spin observables measured in the 500 MeV Los Alamos experiment.[21] This was done at a laboratory scattering angle of 18.5° ($q \approx 300$ MeV/c). The cross section, shown in Fig. 5, peaks at about $\omega = 66$ MeV. First, the polarization was found experimentally to be equal to the analyzing power (within errors). Although not required for the inelastic reaction, this agrees with our model.

However, the analyzing power at the quasielastic peak is 40% below the free NN value both for ^{208}Pb, Fig. 5, and ^{40}Ca, Fig. 6. This reduction in A_y is reproduced by our model and may be a clear relativistic signature. To our knowledge, no nonrelativistic calculation has explained this low value for A_y. The arrows in Fig. 5 are the estimates of **L·S** distortion effects from Ref. 13. Although these do reduce A_y, the **L·S** estimates alone are much smaller than the reduction seen in the data.

It is important to emphasize that all nonrelativistic cal-

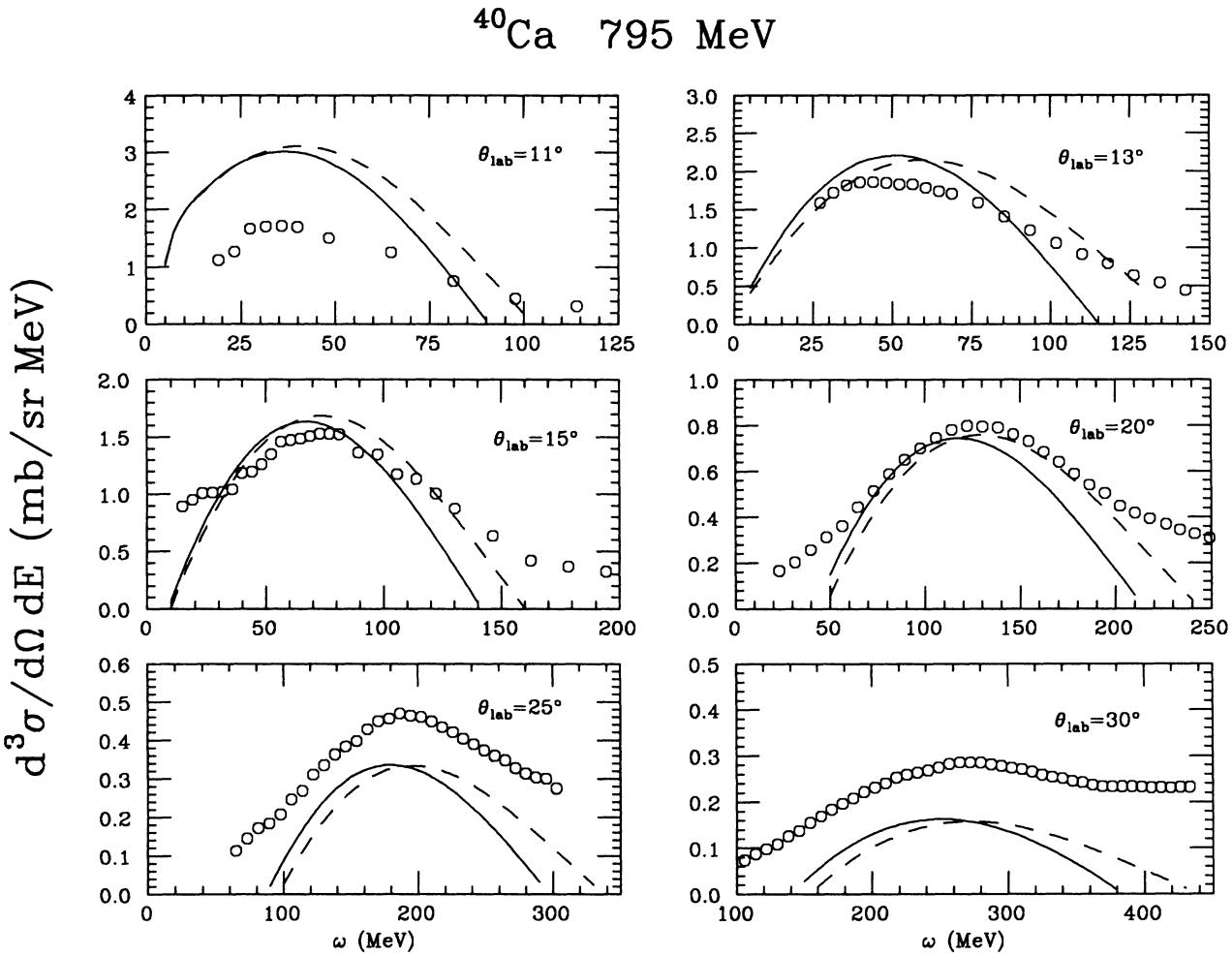

FIG. 3. Same as Fig. 2, but for (p,p′) scattering on ^{40}Ca. Data are from Ref. 12.

culations to date predict the analyzing power to be very close to the free value (within 10%) at the center of the quasielastic peak. Given the high excitation energy $\omega \approx 70$ MeV, nuclear structure correlations are small. Thus the reduction in A_y at the peak is very hard to explain in nonrelativistic models (without changing the interaction).

For ^{208}Pb, the slope of A_y with ω is not reproduced by the calculation. The rise in A_y at very small ω is likely due to nuclear structure effects. Nonrelativistic calculations[29] based on the RPA surface response of Bertsch *et al.*[30] reproduce the rise in A_y with decreasing ω. However, the RPA corrections alone are much too small at $\omega = 66$ MeV to explain the large reduction at the quasifree peak. Furthermore, the slope in A_y may have contributions from multiple scattering or distortion effects. These should be bigger in ^{208}Pb than in ^{40}Ca. Indeed, A_y does not have as steep a slope for Ca as it does for Pb (though the low ω data is missing). Furthermore, some indication of these effects in Pb is suggested by the much broader 800 MeV cross section for Pb compared to Ca or our calculation.

The other polarization transfer coefficients $D_{i'j}$ are shown in Fig. 5 for Pb and Fig. 6 for Ca. For Pb, D_{nn} is reduced somewhat from the free value, in agreement with our M^* predictions. On the other hand, both $D_{l'l}$ and $D_{s's}$ are close to the free values. This disagrees with our M^* calculations which predict an enhancement. However, this increase may be canceled by the $\mathbf{L}\cdot\mathbf{S}$ distortions. These were estimated in Ref. 13 to reduce both $D_{l'l}$ and $D_{s's}$.

Alternatively, our simple mass M^* Fermi gas may be in error. Self-consistency corrections (which we ignore) have been shown to remove the naive M^* enhancements in convection currents and magnetic moments.[31] This may be an important point and needs further study. Such self-consistency corrections can be incorporated with relativistic RPA calculations of the target response where one includes positive and negative-energy mixing.

For $D_{s'l}$ we find only small M^* effects. This disagrees somewhat with Ref. 13 where we found a larger M^* change. This appears to be washed out when we now include the Fermi-motion averaging. The data is also close to the free value.

It is interesting to investigate if relativistic effects are coming from the projectile or target wave function. For

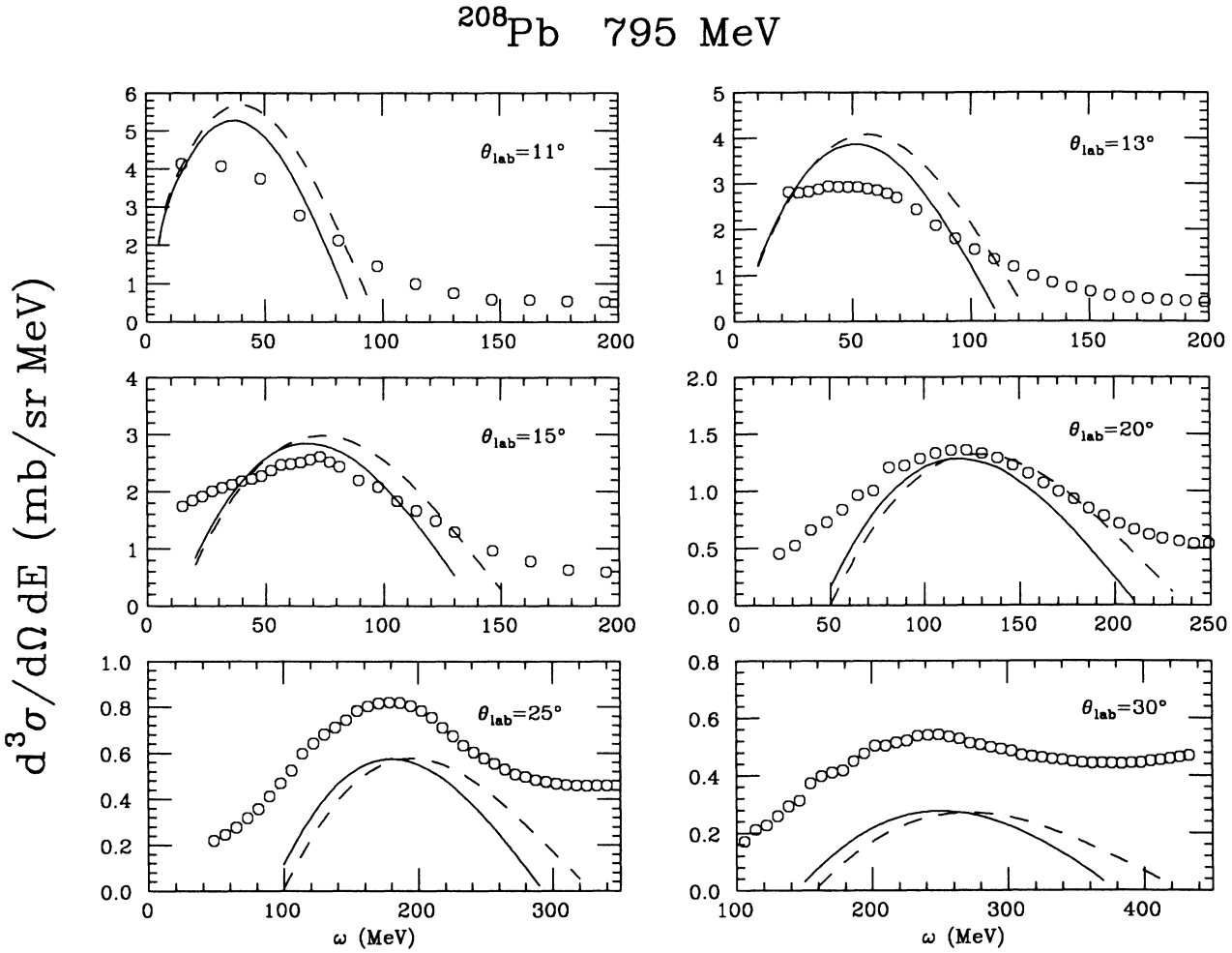

FIG. 4. Same as Fig. 2, but for (p,p') scattering on ^{208}Pb. Data are from Ref. 12.

elastic scattering it has been claimed[20] that most of the change is from the projectile. In Figs. 5 and 6 we also show calculations including only projectile relativity, $M_2=M\neq M_1$, and only target relativity, $M_1=M\neq M_2$. The bulk of the reduction in A_y is seen to come from the projectile wave function. However, for $D_{s'l}$ the two effects are comparable in magnitude and tend to cancel. Thus there are spin observables which may be sensitive to the relativistic nature of the target.

Next, predictions are made at lower energies 300 MeV and 400 MeV in Figs. 7–11. At 400 MeV there are large changes in $D_{s's}$ and $D_{s'l}$ at $\theta_{\rm lab}=10°$. Likewise there are big changes in $D_{s's}$ and $D_{s'l}$ at 300 MeV and forward angles. Note, at lower energies one should consider exchange and other corrections to the simple impulse approximation.[18,24]

C. 500–800 MeV (p,n)

Calculations for quasielastic (p,n) charge-exchange reactions are presented in Fig. 12 for $T_{\rm lab}=795$ MeV and Fig. 13 for 500 MeV. These depend on the isovector NN amplitudes, Eq. (2.38), which are very different from the isoscalar Lorentz invariants, Eq. (2.39). This is illustrated in Table III where the isovector amplitudes no longer have very large scalar and vector parts. Instead they are dominated by the pseudoscalar invariant.

Thus a proper treatment of pion exchange, which gives the pseudoscalar invariant, is crucial for the (p,n) reaction. This is beyond the scope of the present work. Instead we illustrate results for two very simple models.

The first, which we call "pseudoscalar," simply uses the five amplitudes in Table I unmodified. This form is successful for high-energy elastic scattering. However, we emphasize that Table I is not unique.[32] Furthermore, elastic scattering does not test the pseudoscalar invariant directly (since its contribution vanishes by parity). Worse than that, the exchange contribution of the pion to elastic scattering gives problems in this pseudoscalar model at low energies.[19]

Alternatively, for a pseudovector model we replace the γ_5 invariant of Table I with

$$\lambda_{\rm pv}=\frac{\not{q}\gamma_5}{2M}\ , \tag{3.3}$$

where q is the four momentum transfer of Eq. (2.34). For free spinors of mass M, Eq. (3.3) gives the same matrix

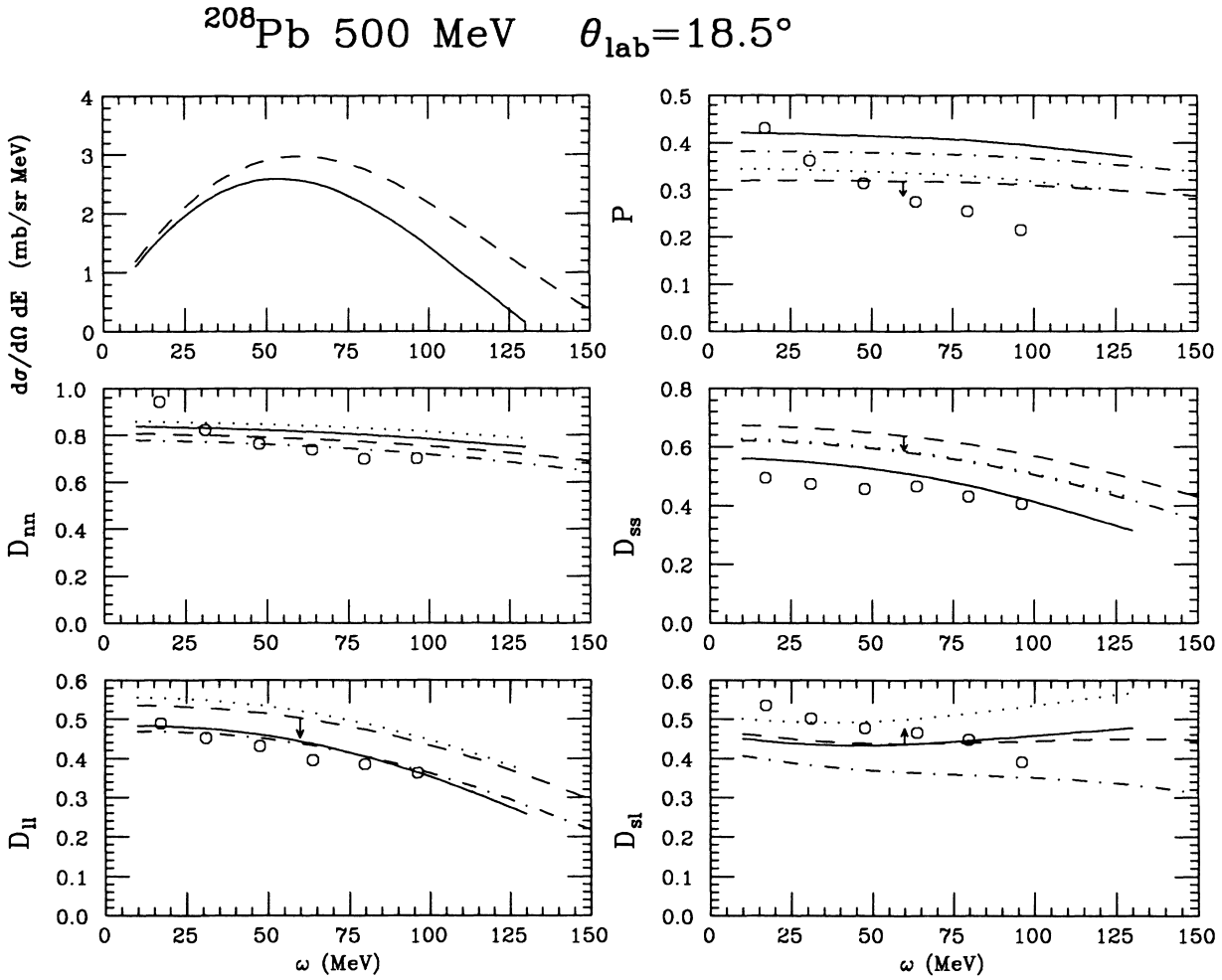

FIG. 5. Cross section and spin observables for (p,p') scattering on ^{208}Pb at 500 MeV, $\theta_{lab}=18.5°$. Solid curves use free masses, $M_1=M_2=M$. Dashed curves use relativistic effective masses for M_1 and M_2. Dotted curve includes only projectile relativity, $M_1\neq M_2=M$. Dotted-dashed curves include only target relativity, $M_2\neq M_1=M$. Data are from Ref. 22.

elements as the original choice

$$\lambda_p=\gamma_5 \ . \tag{3.4}$$

Thus the fit to the NN data is unchanged. However, in the medium,

$$\bar{U}_1(k_1)\lambda_{pv}U_1(p_1)=\frac{M_1}{M}\bar{U}_1(k_1)\lambda_p U_1(p_1) \ , \tag{3.5}$$

which differs by a factor of M_1/M. In the limit $M_1=0$, λ_p gives a very large contribution and λ_{pv} gives zero. For the pseudovector model we simply multiply F_p by

$$F_{pv}=\frac{(M_1M_2)}{M^2}F_p \tag{3.6}$$

to get a "pseudovector" amplitude F_{pv}.

Figure 12 shows that the (p,n) cross section is larger for pseudoscalar than pseudovector calculations. [Note, we have simply added the charge-exchange Q value (=18.1 MeV) to the energy loss ω in Figs. 12 and 13.] One can take the ratio of the maximum in the (p,n) cross section to that of (p,p') in order to cancel the (common?) distortion effects. This ratio is 0.15 ($M_1=M_2=M$), 0.16 (pseudoscalar), and 0.11 (pseudovector) for scattering from ^{12}C at $T_{lab}=800$ MeV and $\theta_{lab}=15°$. It would be useful to have absolute, or ratio to (p,p'), quasifree cross sections measured accurately. The preliminary Los Alamos ^{12}C(p,n) cross sections[33] would suggest pseudoscalar coupling, but they are at a rather small angle (9°) and there may be uncertainties in A_{eff}.

The spin observables in Figs. 12 and 13 are also sensitive to the form of the pion coupling. Although A_y and $D_{s'l}$ do not change much, D_{nn} and $D_{s's}$ are dramatically different. For (p,p') scattering (not shown) there is much less sensitivity to the form of the pseudoscalar invariant.

D. Test of Fermi gas model

All of our calculations have been based on a local Fermi gas approximation. To test this we make a different local density approximation. In the calculation of Sec. II, effective parameters are obtained by averaging over local

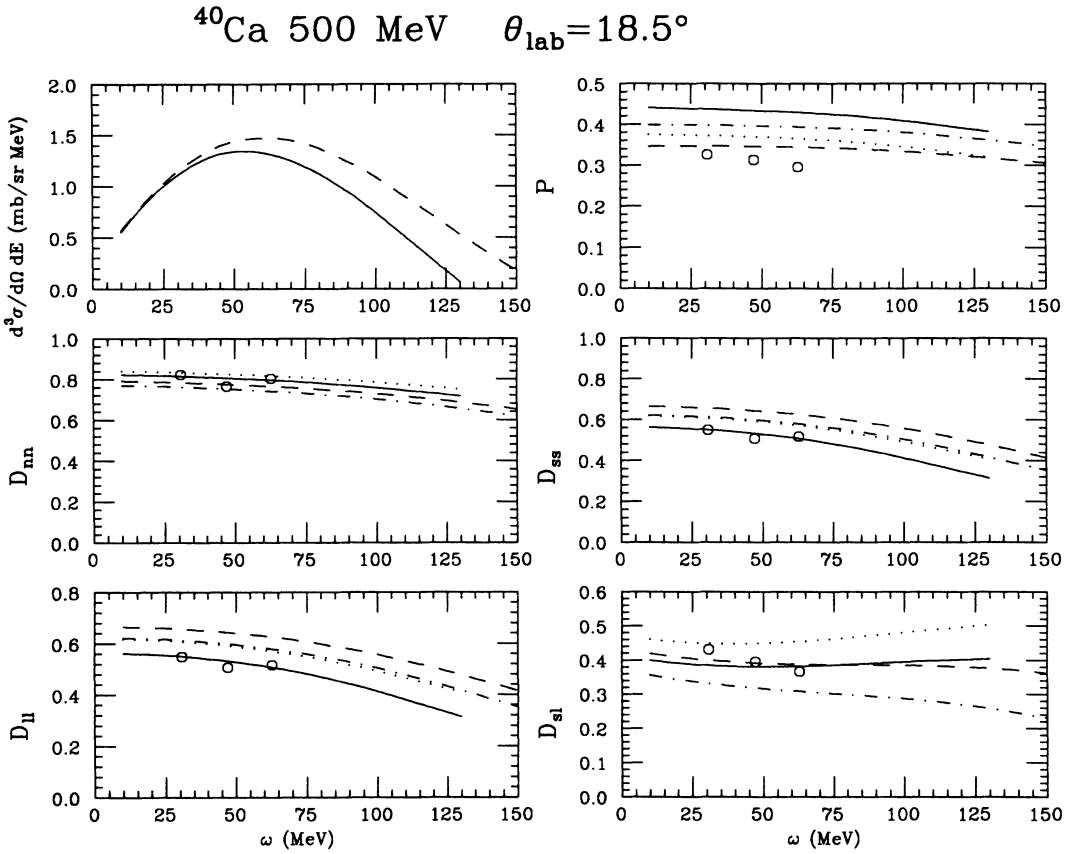

FIG. 6. Same as Fig. 5, but for (p,p′) scattering on ^{40}Ca. Data are from Ref. 22.

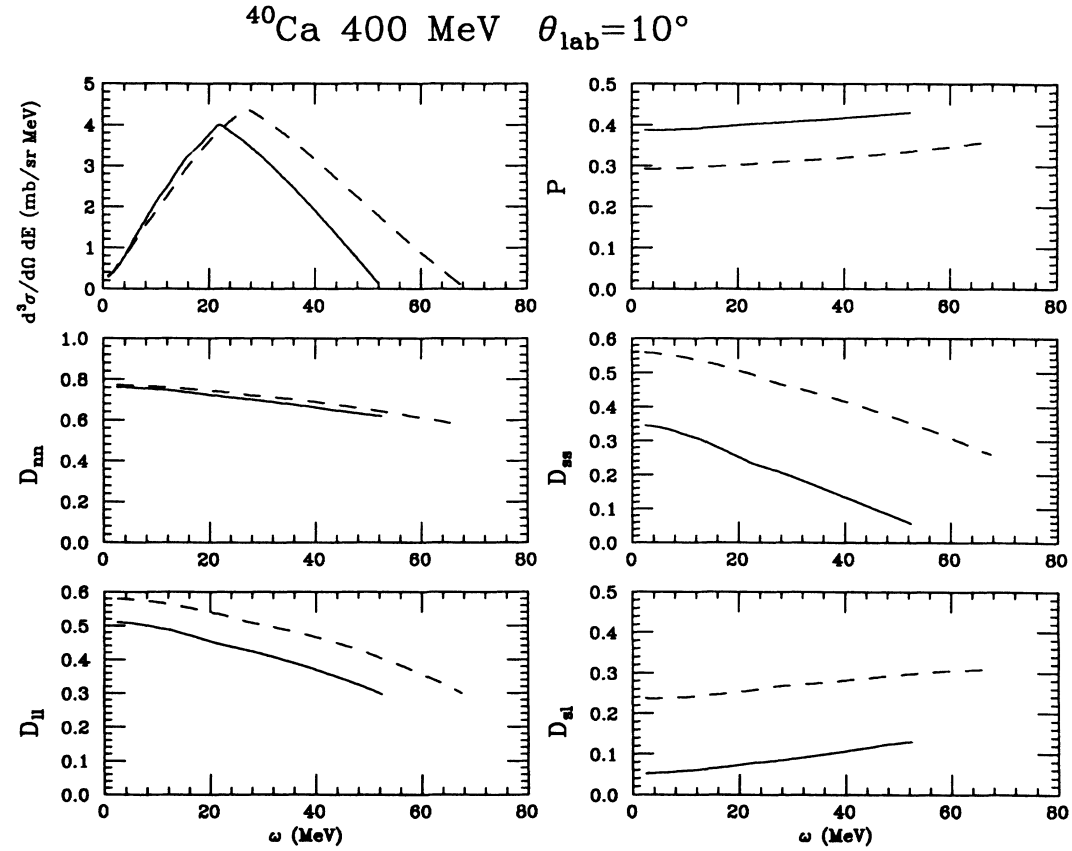

FIG. 7. Scattering observables for (p,p′) scattering on Ca at 400 MeV, at θ_{lab}=10°.

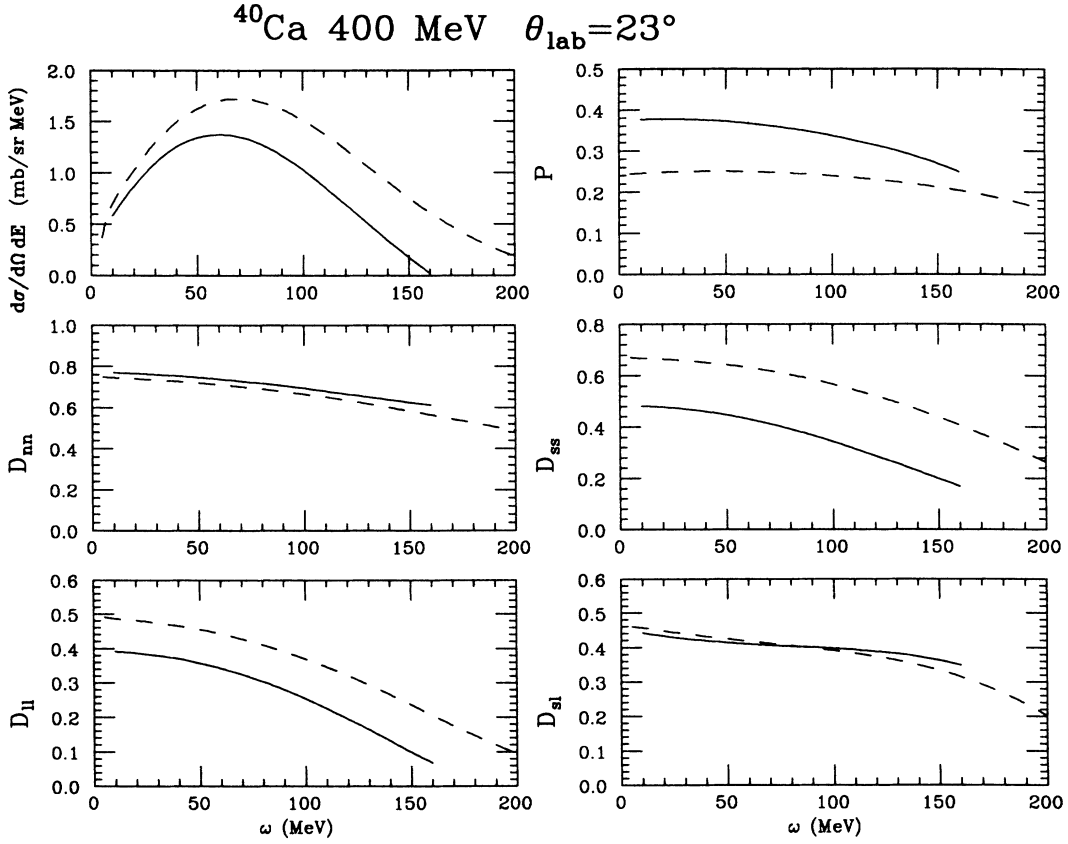

FIG. 8. Same as Fig. 7, but for scattering at $\theta_{lab}=23°$.

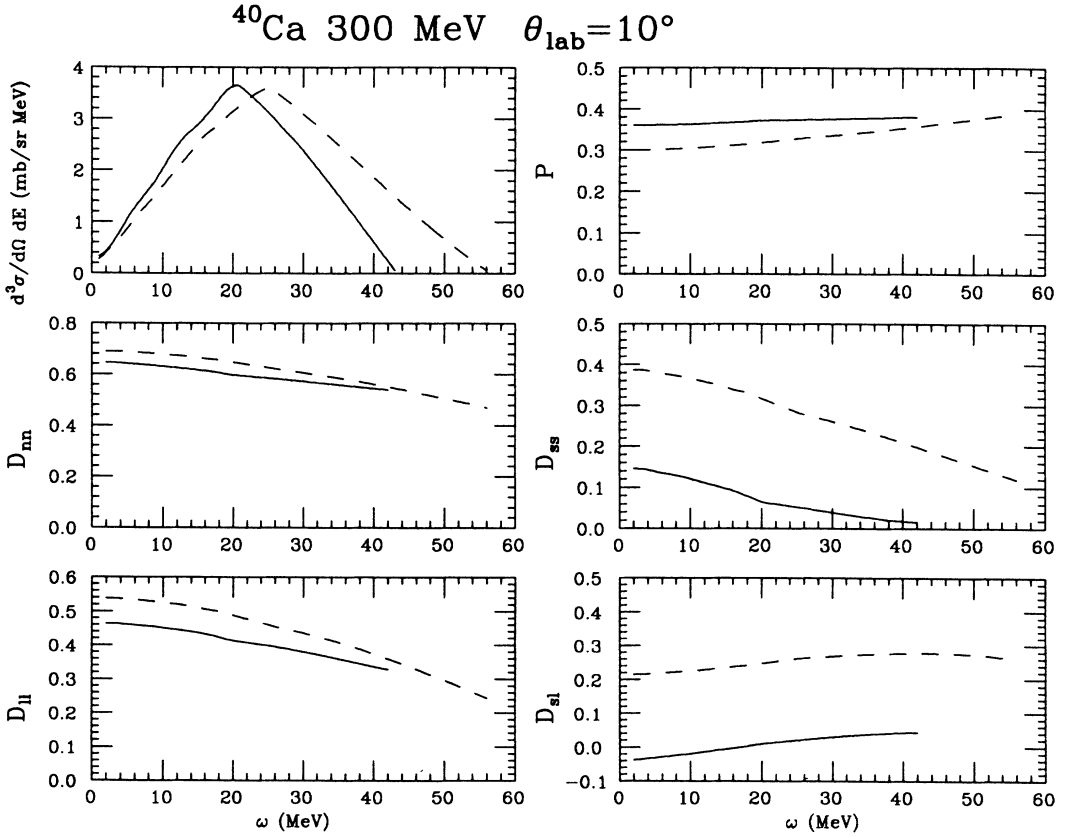

FIG. 9. Observables for (p,p′) scattering on ^{40}Ca at 300 MeV at $\theta_{lab}=10°$. The solid curve uses $M_1=M_2=M$. The dashed curve uses relativistic effective masses for M_1 and M_2.

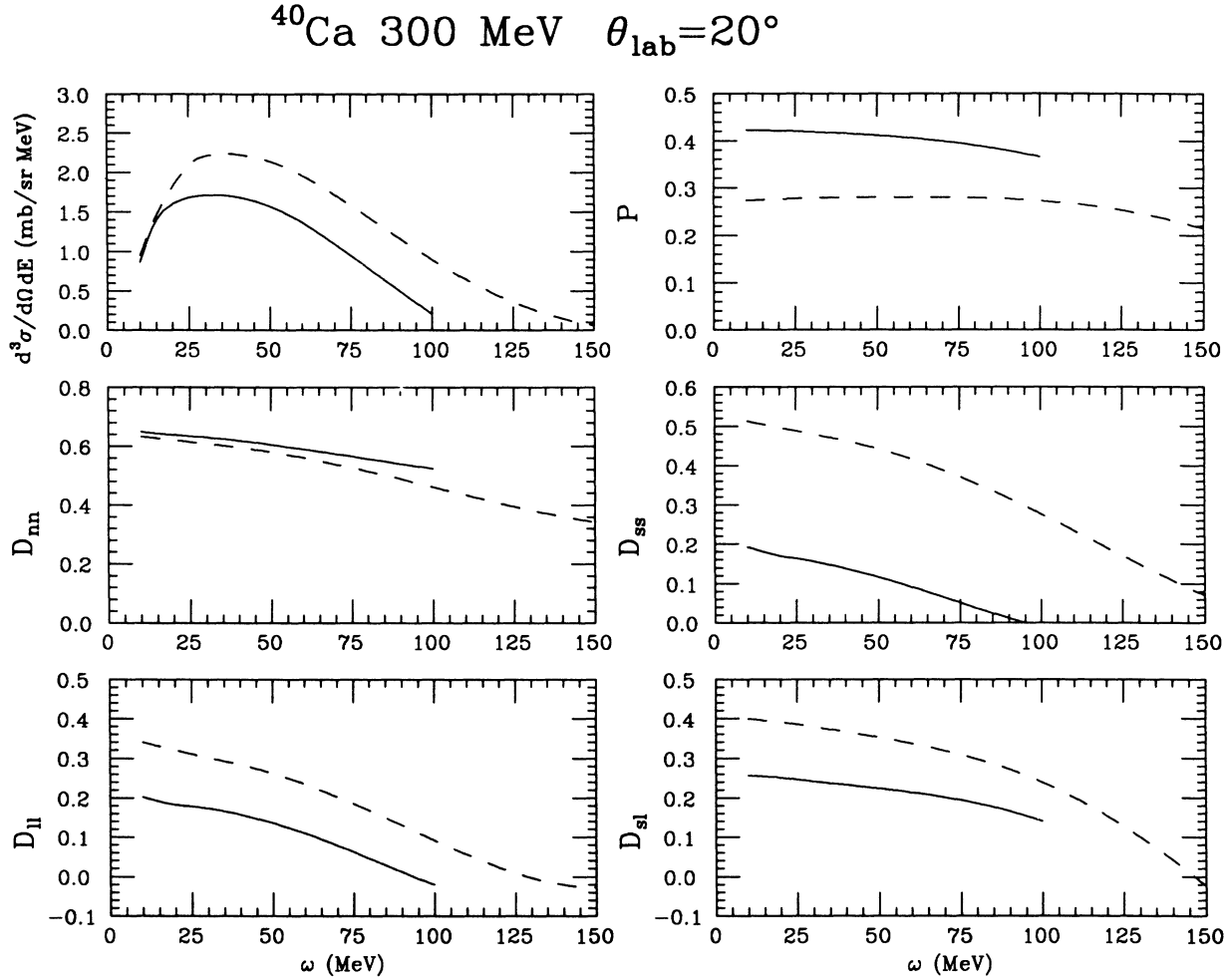

FIG. 10. Same as Fig. 9, but for scattering at $\theta_{lab}=20°$.

values in the nucleus *first*. Another approach to the calculation would be to perform this averaging afterward, that is, calculating the scattering observables for the *local* Fermi gas parameters and then averaging these over the nuclear volume. This calculation proceeds as follows.

Define local values of k_F, M_1, and M_2 by

$$k_F(r)=[\tfrac{3}{2}\pi^2\rho_B(r)]^{1/3}\ , \tag{3.7a}$$

$$M_1(r)=M-S(r),\quad M_2(r)=M-0.44\frac{\rho(r)}{\rho_0}\ . \tag{3.7b}$$

We use these values in Eqs. (2.24) and (2.26) to get local cross sections and then average the result:

$$\frac{d^3\sigma}{d\Omega_1' dE_1'}=\int b\,db\int dz\,T(b)\left[\rho_p(r)\frac{d^3\sigma(\mathrm{pp})}{d\Omega_1' dE_1'}(M_1(r),M_2(r),k_F(r))+\rho_n(r)\frac{d^3\sigma(\mathrm{pn})}{d\Omega_1' dE_1'}(M_1(r),M_2(r),k_F(r))\right]\ . \tag{3.8}$$

The spin observables are calculated in a similar fashion.

Calculations using both averaging schemes are compared in Fig. 14 for 800 MeV proton scattering on ^{40}Ca at $\theta_{lab}=20°$. The dashed curves are calculated using Eqs. (3.7) and (3.8). The solid curves are the corresponding nonrelativistic calculation, using $M_1=M_2=M$ in place of (3.7b).

Comparing these results to the data and the calculation of Sec. II (the dashed-dotted and dotted curves in Fig. 14), the cross section is too sharply peaked, and there is a change in the shapes of the spin observables. The averaging scheme of Eq. (3.8) gives a contribution from the nuclear surface where the local k_F is low. For very low k_F, a Fermi gas may be a bad approximation to the nuclear surface, especially when the local Fermi wavelength is much larger than the surface thickness. Therefore the spike at the center of the quasielastic peak, which comes from these low-momentum contributions, may be spuri-

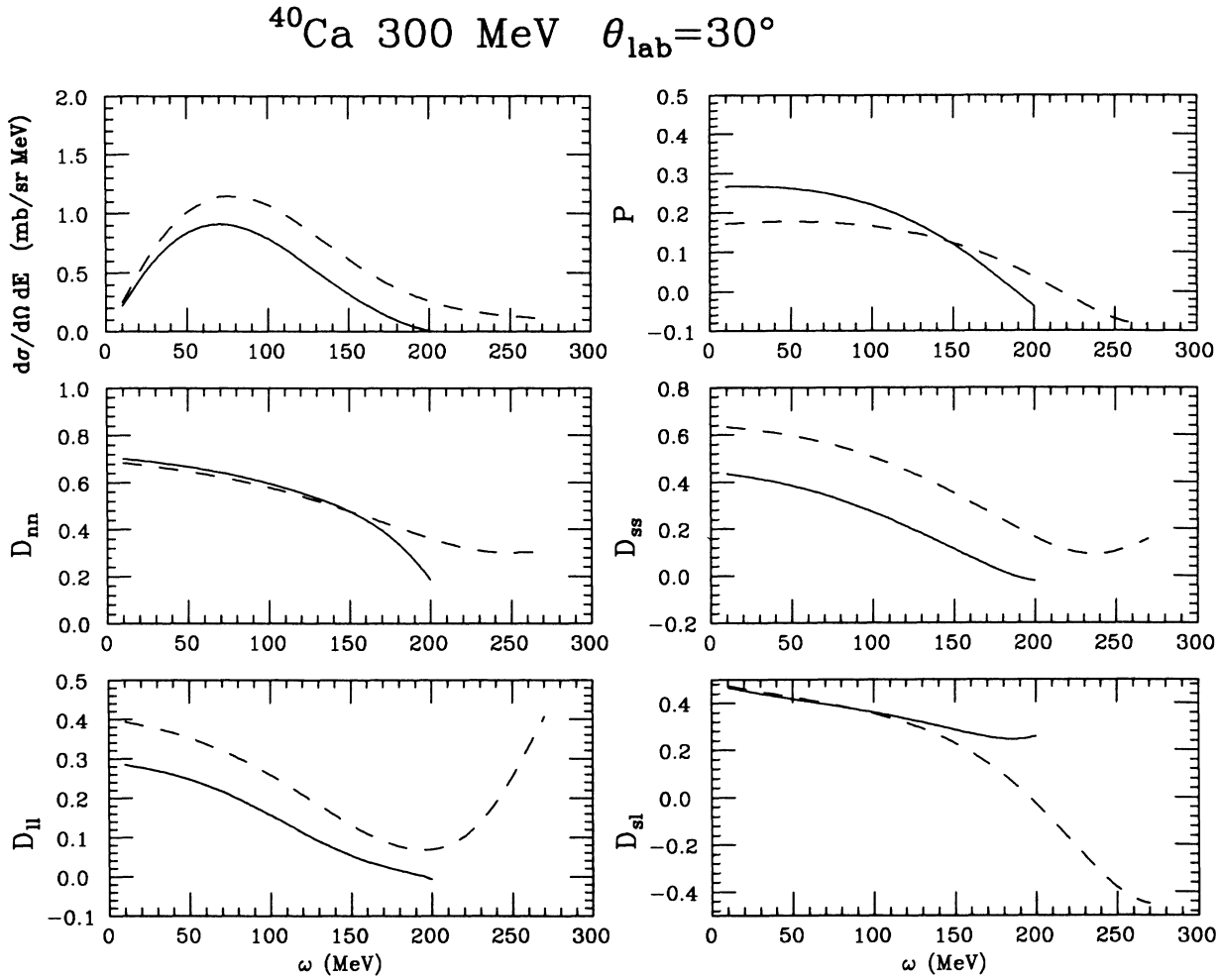

FIG. 11. Same as Fig. 9, but for scattering at $\theta_{lab}=30°$.

ous. However, even with these changes to the cross section, the spin observables for the peak are similar. Therefore, qualitative features such as the relativistic decrease in A_y are probably not sensitive to the averaging procedure employed.

IV. SUMMARY

In this paper a relativistic plane-wave impulse approximation (RPWIA) was developed for quasielastic proton-nucleus scattering. Quasielastic scattering is fundamental since the reactive content of impulse approximations used for elastic scattering is quasifree single-nucleon knockout. Furthermore, the spin observables in proton scattering are as basic information about the nuclear medium as are the longitudinal and transverse responses of quasielastic electron scattering.

We have assumed a relativistic Fermi gas model for the target in a local density approximation, either at one average density or integrated over the local density at each point in the nucleus. This should be an adequate representation of the nuclear structure except at very low excitation energy (say, $\lesssim 30$ MeV).

We have focused on a change in the NN interaction in the medium coming from modified nucleon Dirac spinors. These spinors have enhanced lower components from the strong scalar optical potential and can be characterized by the value of M^*. For the somewhat surface peaked quasielastic reaction we have used an average value of M^*/M of 0.8–0.9.

The spinors are used to take matrix elements of the relativistic NN t matrix, $\hat{\mathcal{F}}$, which is assumed to be a Dirac operator in the spinor space of the two nucleons. *Any model for $\hat{\mathcal{F}}$ makes definite predictions of how NN spin-observables in quasielastic scattering will change as M^* decreases.* Here we have used the simple five term S, V, T, P, A amplitudes of Table I which have been successfully employed in elastic scattering.

As M^* decreases there are only small changes in the cross section. Furthermore, these small changes may be masked by uncertainties in distortions. Therefore we find *no clear relativistic signatures in the unpolarized (p,p') quasifree cross section.*

In contrast, the analyzing power A_y is found to decrease substantially. Basically, the spin-orbit interaction (which involves a coherent sum of S and V) is approximately unchanged with M^* while the central interaction (which involves sensitive cancellations between S and V) increases greatly and "dilutes" A_y.

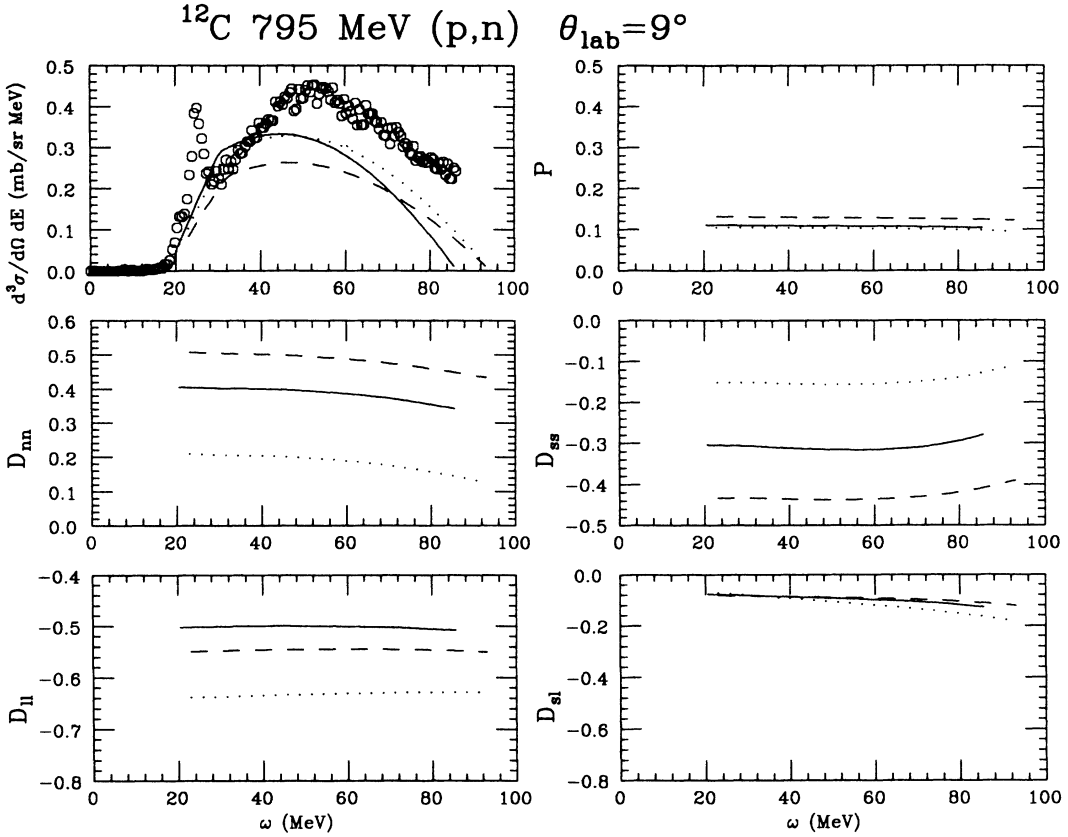

FIG. 12. Cross section and spin observables for (p,n) scattering on ^{12}C at 795 MeV at $\theta_{lab}=9°$. The solid curve uses $M_1=M_2=M$. The dotted curve uses relativistic M's with pseudoscalar coupling. The dashed curve uses relativistic M's with pseudovector coupling. Data are from Ref. 33.

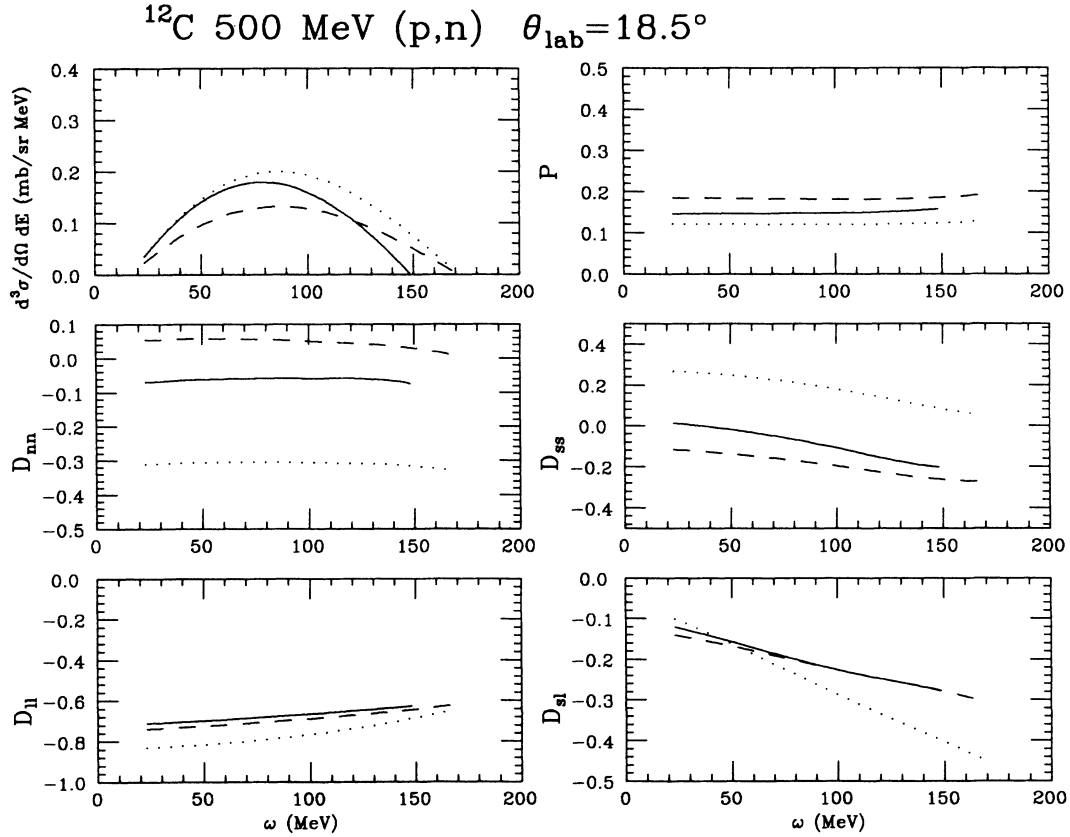

FIG. 13. Same as Fig. 12, but for (p,n) scattering on ^{12}C at 500 MeV and $\theta_{lab}=18.5°$.

TABLE III. Absolute value of isoscalar (top) and isovector NN amplitudes for $T_{lab}=500$ MeV and $\theta_{lab}=18.5°$. The S, V, T, P, and A amplitudes are of the form given in Table I.

i	S	V	T	P	A
$\lvert F_i^{pp}+F_i^{pn}\rvert$ (GeV^{-2})	33.4	23.1	0.99	78.5	2.20
$\lvert F_i^{pp}-F_i^{pn}\rvert$ (GeV^{-2})	3.24	2.04	0.945	477.3	0.144

This decrease in A_y may be the clearest relativistic signature found to date. This is because (a) the background is small and controllable, (b) there is a relatively simple link between relativistic effects on the spinors and changes in A_y, and (c) nonrelativistic calculations all predict essentially the free value of A_y, which provides a clear benchmark for comparison. Furthermore, (to our knowledge) there have been *no alternative explanations* for this decrease in A_y.

The background at the quasielastic peak is estimated to be less than 10%. The effect of spin-orbit distortions on A_y have been found in Ref. 13 and elsewhere to be small for a heavy nucleus (^{208}Pb) and negligible for ^{12}C. Multiple scattering contributions (with two or more hard collisions) are smaller by an order of magnitude in Ref. 14. This work also finds nuclear structure corrections to a Fermi gas are very small at the high excitation energies ($\gtrsim 60$ MeV) of the Los Alamos experiment. Furthermore, there are other spin observables (with small relativistic corrections) which are measured to be close to their free values. This severely constrains possible sources of background.

In our calculations, the link between changes in the spinors and changes in A_y is relatively direct. A_y is dominated by the t_S and t_V amplitudes; at very small angles A_y can be approximated by

$$A_y \approx \frac{p_1^2 \mathrm{Im}[t_S^* t_V]\sin\theta_{lab}}{|M_1 t_S + E_1^* t_V|^2}\ , \tag{4.1}$$

showing that the decrease in A_y with decreasing M^* arises from a very sensitive cancellation between the scalar and vector amplitudes. (The origin of the M^* effect for the other spin observables is less direct; for example, the large differences in D_{nn} in Fig. 13 come from the pseudoscalar amplitude which gives no contribution in this small-angle approximation.) In contrast, the relativistic effects found in elastic scattering involve a complex

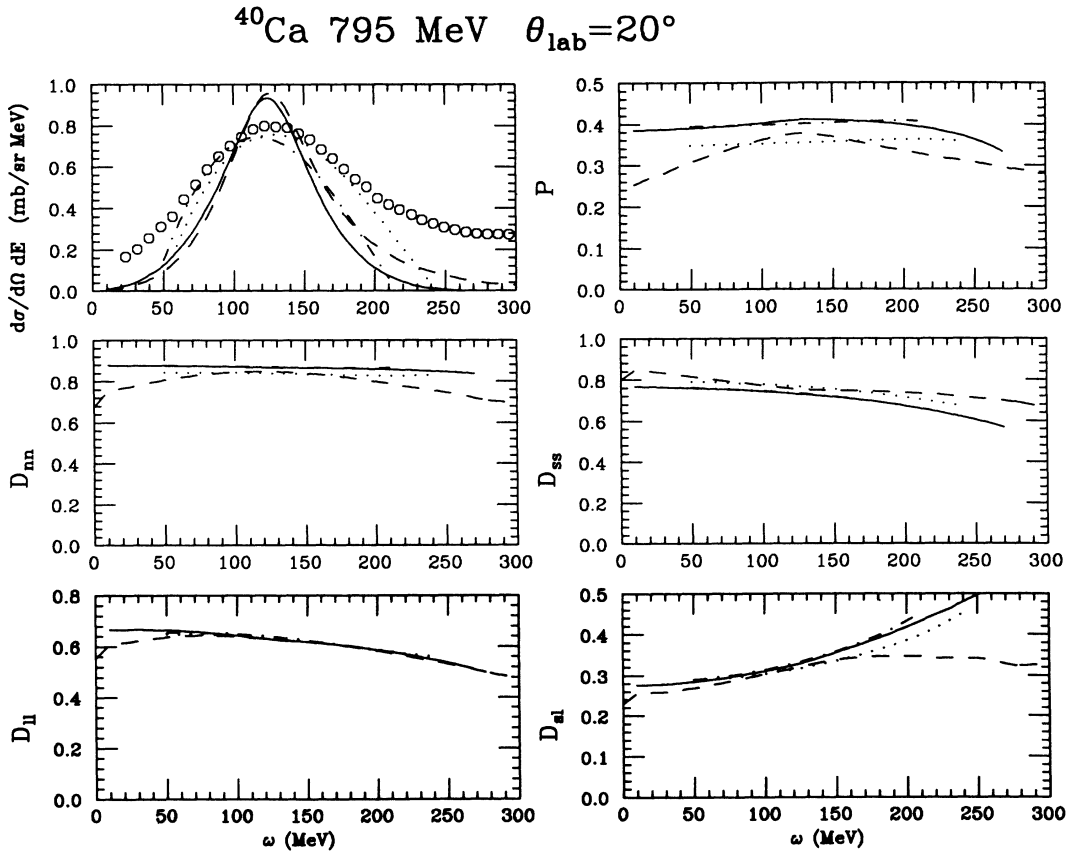

FIG. 14. Observables for (p,p′) scattering on ^{40}Ca at 795 MeV and $\theta_{lab}=20°$. The dashed-dotted and dotted curves are the nonrelativistic and relativistic calculations using effective parameters as described in Sec. II. The solid and dashed curves are nonrelativistic and relativistic calculations using the local density averaging scheme of Sec. IV, Eqs. (3.7) and (3.8).

interplay of several effects. There is no simple relationship between the spin observables A_y and Q in forward angle diffraction minima and parts of the NN t matrix or relativistic wave functions.

The experimental situation for A_y at the top of the quasielastic peak is clear. A_y or P is found to be below the free value for a variety of nuclei and energies. Perhaps the largest reduction, of approximately 40%, was found for ^{40}Ca and ^{208}Pb in the 500 MeV Los Alamos experiment.[21]

Relativistic effects for the polarization-transfer coefficients $D_{i'j}$ at 500 MeV are predicted to be small. First, the off-diagonal observables $D_{l's}$ and $D_{s'l}$ are predicted to be virtually unchanged with M^*. Experimentally[21] these are close to their free values in ^{40}Ca and ^{208}Pb at 500 MeV.

Second, $D_{l'l}$ and $D_{s's}$ rise somewhat with decreasing M^*. However, $\mathbf{L}\cdot\mathbf{S}$ distortion in heavy nucleus may cancel much of the increase. This could explain why the measurements in Ref. 21 are close to the free values of $D_{l'l}$ and $D_{s's}$. Thus at 500 MeV there are no polarization-transfer observables with clear relativistic changes. However, the "null" results of Ref. 21 could still be consistent with our model if there is some cancellation between relativistic and $\mathbf{L}\cdot\mathbf{S}$ effects.

As the energy decreases to 300 or 400 MeV, relativistic effects on $D_{i'j}$ are found to be larger. Furthermore, the cancelling background from the $\mathbf{L}\cdot\mathbf{S}$ potential is much smaller in a light nucleus such as ^{12}C or ^{16}O. Therefore, the $D_{i'j}$'s should be measured for energies below 500 MeV in a nucleus lighter than ^{40}Ca.

The charge exchange (p,n) reaction presents a completely different picture. Here one looks at relativistic effects in the isovector NN amplitudes. Because these do not involve sensitive cancellations between t_S and t_V the analyzing power A_y changes only slightly with M^*. Instead the pseudoscalar invariant from pion exchange dominates. The cross section, D_{nn}, $D_{s's}$, and $D_{l'l}$ all change greatly with M^* and depend on how one treats the pion.

Therefore, the ratio of (p,n) to (p,p') cross sections should be measured along with any experimentally accessible $D_{i'j}$. However, we emphasize that our calculations are based on extremely crude pseudovector and pseudoscalar treatments of the pion. More sophisticated theoretical calculations are clearly needed, and these might not show such large relativistic effects.

Much remains to be done both theoretically and experimentally. Full relativistic DWIA calculations should be done to confirm our local density approximation and look at $\mathbf{L}\cdot\mathbf{S}$ effects. Also, relativistic RPA calculations of the nuclear response are needed to examine both particle-hole corrections to the nuclear structure (at low energies) and positive- and negative-energy mixing. These mixing or "backflow" corrections are known to be important in relativistic calculations of convection currents.

In addition, calculations for more sophisticated models of $\hat{\mathcal{F}}$ beyond our simple five term representation would be useful. Furthermore, at low energies one needs to consider corrections to our RPWIA from Pauli blocking and explicit treatments of nucleon exchange.

More experimental data is needed for a range of energies, targets and scattering angles. Any individual polarization transfer coefficient is interesting even if it is not possible to measure a complete set. However, because one is interested in (perhaps) small changes from free values it would be useful to have as accurate a measurement as possible. Finally, the ratio of (p,p') to (p,n) cross sections should be measured.

ACKNOWLEDGMENTS

This work was supported in part under the U.S. Department of Energy Contract Nos. DE-AC02-76-ER03069 (Massachusetts Institute of Technology) and DE-AC02-81-ER40047 (Indiana University Cyclotron Facility), and by a Chester Davis Fellowship.

APPENDIX: EXPRESSIONS FOR SPIN OBSERVABLES

The terms in $\sum_{s_2,s_2'}\mathcal{M}^*\mathcal{M}$ which are proportional to $s_i\cdot s_f$ are listed first. Define

$$\begin{aligned}\mathcal{S}\equiv -s_i\cdot s_f[&t_S^*t_S(1+K_1\cdot P_1)(1+K_2\cdot P_2)-t_P^*t_P(1-K_1\cdot P_1)(1-K_2\cdot P_2)\\&+2(t_V^*t_V-t_A^*t_A)(1+K_1\cdot K_2P_1\cdot P_2-K_1\cdot P_1K_2\cdot P_2+K_1\cdot P_2K_2\cdot P_1)-8t_T^*t_T(K_1\cdot P_1+K_2\cdot P_2)\\&+2\,\mathrm{Re}(t_V^*t_S+2t_T^*t_A)(K_1\cdot K_2+K_1\cdot P_2+K_2\cdot P_1+P_1\cdot P_2)\\&+4\,\mathrm{Re}(t_T^*t_P-t_T^*t_S)(K_1\cdot K_2P_1\cdot P_2-K_1\cdot P_2K_2\cdot P_1)\\&+2\,\mathrm{Re}(t_A^*t_P+2t_T^*t_V)(K_1\cdot P_2+K_2\cdot P_1-K_1\cdot K_2-P_1\cdot P_2)]\ .\end{aligned}\tag{A1}$$

Then the squared amplitude summed over the initial and final spins of the struck nucleon is given by

$$
\begin{aligned}
4\sum_{s_2,s_2'}\mathcal{M}^*\mathcal{M} = {} & \mathcal{S}+t_S^*t_S(1+K_2\cdot P_2)s_i\cdot K_1 s_f\cdot P_1+t_P^*t_P(1-K_2\cdot P_2)s_i\cdot K_1 s_f\cdot P_1 \\
& +2t_V^*t_V[s_i\cdot K_1 s_f\cdot K_2 P_1\cdot P_2+s_f\cdot P_1 s_i\cdot K_2 K_1\cdot P_2-s_f\cdot P_1 s_i\cdot K_1 K_2\cdot P_2 \\
& \quad +(1-K_1\cdot P_1)(s_f\cdot K_2 s_i\cdot P_2+s_i\cdot K_2 s_f\cdot P_2)+s_f\cdot P_2 s_i\cdot K_1 K_2\cdot P_1+s_i\cdot P_2 s_f\cdot P_1 K_1\cdot K_2] \\
& +2t_A^*t_A[s_i\cdot K_1 s_f\cdot P_1 K_2\cdot P_2-s_i\cdot K_1 s_f\cdot K_2 P_1\cdot P_2-s_i\cdot K_1 s_f\cdot P_2 K_2\cdot P_1 \\
& \quad +(1+K_1\cdot P_1)(s_i\cdot K_2 s_f\cdot P_2+s_f\cdot K_2 s_i\cdot P_2)-s_f\cdot P_1 s_i\cdot P_2 K_1\cdot K_2-s_i\cdot K_2 s_f\cdot P_1 K_1\cdot P_2] \\
& -8t_T^*t_T[s_i\cdot K_1 s_f\cdot P_1+2(s_i\cdot K_2 s_f\cdot P_2+s_i\cdot P_2 s_f\cdot K_2)] \\
& +2\,\mathrm{Re}(t_V^*t_S+2t_T^*t_A)(s_i\cdot K_1 s_f\cdot K_2+s_f\cdot P_1 s_i\cdot K_2+s_f\cdot P_2 s_i\cdot K_1+s_i\cdot P_2 s_f\cdot P_1) \\
& +2\,\mathrm{Re}(t_A^*t_P+2t_T^*t_V)(s_i\cdot K_1 s_f\cdot P_2+s_f\cdot P_1 s_i\cdot K_2-s_f\cdot K_2 s_i\cdot K_1-s_i\cdot P_2 s_f\cdot P_1) \\
& +4\,\mathrm{Re}(t_A^*t_V)(s_i\cdot P_2 s_f\cdot K_2-s_i\cdot K_2 s_f\cdot P_2) \\
& +4\,\mathrm{Re}(t_T^*t_S)[(1+K_1\cdot P_1)(s_f\cdot K_2 s_i\cdot P_2-s_i\cdot K_2 s_f\cdot P_2)-K_1\cdot K_2 s_f\cdot P_1 s_i\cdot P_2 \\
& \quad +K_1\cdot P_2 s_i\cdot K_2 s_f\cdot P_1+K_2\cdot P_1 s_i\cdot K_1 s_f\cdot P_2-P_1\cdot P_2 s_i\cdot K_1 s_f\cdot K_2] \\
& +4\,\mathrm{Re}(t_T^*t_P)[(1-K_1\cdot P_1)(s_f\cdot K_2 s_i\cdot P_2-s_f\cdot P_2 s_i\cdot K_2)+K_1\cdot K_2 s_f\cdot P_1 s_i\cdot P_2 \\
& \quad -K_1\cdot P_2 s_i\cdot K_2 s_f\cdot P_1-K_2\cdot P_1 s_i\cdot K_1 s_f\cdot P_2+P_1\cdot P_2 s_i\cdot K_1 s_f\cdot K_2]\ . \qquad \text{(A2)}
\end{aligned}
$$

Because s_i and s_f appear together in every term, the four terms in the definition of $M_{i'j}$, Eq. (2.30a), are all equal.

*Present address: Nuclear Theory Center and Department of Physics, Indiana University, Bloomington, IN 47405.

[1] B. C. Clark. S. Hama, and R. L. Mercer, in *The Interaction Between Medium Energy Nucleons in Nuclei-1982,* Proceedings of the Workshop of the Interaction Between Medium Energy Nucleons in Nuclei, AIP Conf. Proc. No. 97, edited by H. O. Meyer (AIP, New York, 1983).

[2] B. D. Serot and J. D. Walecka, in *Advances in Nuclear Physics,* edited by J. W. Negele and E. Vogt (Plenum, New York, 1986), Vol. 16.

[3] J. A. McNeil, J. R. Shepard, and S. J. Wallace, Phys. Rev. Lett. **50**, 1439 (1983).

[4] J. R. Shepard, J. A. McNeil, and S. J. Wallace, Phys. Rev. Lett. **50**, 1443 (1983).

[5] L. Ray *et al.*, Phys. Rev. Lett. **56**, 2465 (1986).

[6] J. Shepard, in *Proceedings of the LAMPF Workshop on Physics with Polarized Nuclear Targets, Los Alamos National Laboratory, 1986,* LAMPF Conference Report LA-10772-C, edited by G. Burleson, W. Gibbs, G. Hoffmann, J. J. Jarmer, and N. Takeda (Los Alamos National Laboratory, Los Alamos, 1986).

[7] E. Rost and J. R. Shepard, Phys. Rev. C **35**, 681 (1987).

[8] J. R. Shepard, E. Rost, and J. Piekarewicz, Phys. Rev. C **30**, 1604 (1986).

[9] J. R. Shepard, E. Rost, and J. A. McNeil, Phys. Rev. C **33**, 634 (1986).

[10] R. Rosenfelder, Ann. Phys. (N.Y.) **128**, 188 (1980).

[11] A. Picklesimer, J. W. van Orden, and S. J. Wallace, Phys. Rev. C **32**, 1312 (1985).

[12] R. E. Chrien *et al.*, Phys. Rev. C **21**, 1014 (1980).

[13] C. J. Horowitz and M. J. Iqbal, Phys. Rev. C **33**, 2059 (1986).

[14] R. D. Smith and S. J. Wallace, Phys. Rev. C **32**, 1654 (1985).

[15] C. J. Horowitz and B. D. Serot, Nucl. Phys. **A368**, 501 (1981).

[16] C. J. Horowitz and B. D. Serot, Nucl. Phys. **A464**, 613 (1987).

[17] L. Ray and G. W. Hoffmann, Phys. Rev. C **31**, 538 (1985).

[18] D. P. Murdock and C. J. Horowitz, Phys. Rev. C **35**, 1442 (1987).

[19] C. J. Horowitz and B. D. Serot, Phys. Lett. **108B**, 377 (1982).

[20] M. V. Hynes *et al.*, Phys. Rev. Lett. **52**, 978 (1984).

[21] T. Carey *et al.*, Phys. Rev. Lett. **53**, 144 (1984); private communication.

[22] J. D. Bjorken and S. Drell, *Relativistic Quantum Mechanics* (McGraw-Hill, New York, 1964).

[23] J. D. Walecka, Ann. Phys. (N.Y.) **83**, 491 (1974).

[24] C. J. Horowitz, Phys. Rev. C **31**, 1340 (1985).

[25] R. A. Arndt and D. Roper, SAID scattering analysis program (unpublished).

[26] R. Amado *et al.*, Phys. Rev. C **31**, 1340 (1983).

[27] J. A. McGill *et al.*, Phys. Rev. C **29**, 204 (1984).

[28] A. M. Kobos, E. D. Cooper, J. I. Johansson, and H. S. Sherif, Nucl. Phys. **A445**, 605 (1985).

[29] C. Glashausser *et al.*, Phys. Rev. Lett. **58**, 2404 (1987).

[30] H. Esbensen and G. Bertsch, Ann. Phys. (N.Y.) **157**, 255 (1984).

[31] J. A. McNeil *et al.*, Phys. Rev. C **34**, 746 (1986); R. J. Furnstahl and B. D. Serot, Nucl. Phys. **A468**, 539 (1987).

[32] D. L. Adams and M. Bleszynski, Phys. Lett. **136B**, 10 (1984).

[33] R. Jeppesen, Ph.D. thesis, University of Colorado, 1986 (unpublished).